A Novel p38 Mitogen-activated Protein Kinase/Elk-1 Transcription Factor-dependent Molecular Mechanism Underlying Abnormal Endothelial Cell Proliferation in Plexogenic Pulmonary Arterial Hypertension[*]

Monal Patel[‡], Dan Predescu[‡], Rajive Tandon[‡], Cristina Bardita[‡], Jennifer Pogoriler[§], Sangeeta Bhorade[¶], Minhua Wang[‡], Suzy Comhair[∥], Anna Ryan-Hemnes[**], Jiwang Chen[‡‡], Roberto Machado[‡‡], Aliya Husain[§], Serpil Erzurum[∥], and Sanda Predescu[‡1]

From the ‡Departments of Pharmacology and Medicine, Vascular Biology, and Pulmonary and Critical Care Medicine, Rush University Medical Center, Chicago, Illinois 60612, §Department of Pathology and ¶Center for Lung Transplant, University of Chicago, Chicago, Illinois 60637, ∥Department of Pathobiology, Lerner Research Institute, Cleveland Clinic, Cleveland, Ohio 44195, **Division of Allergy, Pulmonary, and Critical Care Medicine, Vanderbilt University, Nashville, Tennessee 37240, and ‡‡Section of Pulmonary, Critical Care Medicine, Sleep and Allergy, University of Illinois, Chicago, Illinois 60612

Background: Plexiform lesions comprising proliferative endothelial cells are hallmarks of pulmonary arterial hypertension.
Results: Granzyme B cleaves intersectin-1s and generates a fragment with endothelial cell proliferative potential via phosphorylation of p38^{MAPK} and Elk-1 transcription factor.
Conclusion: Granzyme B cleavage of intersectin-1s and subsequent p38^{MAPK}/Elk-1 activation are critical for endothelial cell proliferation.
Significance: The novel pathogenic p38^{MAPK}/Elk-1 signaling may explain the formation of plexiform lesions.

Plexiform lesions (PLs), the hallmark of plexogenic pulmonary arterial hypertension (PAH), contain phenotypically altered, proliferative endothelial cells (ECs). The molecular mechanism that contributes to EC proliferation and formation of PLs is poorly understood. We now show that a decrease in intersectin-1s (ITSN-1s) expression due to granzyme B (GrB) cleavage during inflammation associated with PAH and the high p38/Erk1/2^{MAPK} activity ratio caused by the GrB/ITSN cleavage products lead to EC proliferation and selection of a proliferative/plexiform EC phenotype. We used human pulmonary artery ECs of PAH subjects (EC$_{PAH}$), paraffin-embedded and frozen human lung tissue, and animal models of PAH in conjunction with microscopy imaging, biochemical, and molecular biology approaches to demonstrate that GrB cleaves ITSN-1s, a prosurvival protein of lung ECs, and generates two biologically active fragments, an N-terminal fragment (GrB-EH$_{ITSN}$) with EC proliferative potential and a C-terminal product with dominant negative effects on Ras/Erk1/2. The proliferative potential of GrB-EH$_{ITSN}$ is mediated via sustained phosphorylation of p38^{MAPK} and Elk-1 transcription factor and abolished by chemical inhibition of p38^{MAPK}. Moreover, lung tissue of PAH animal models and human specimens and EC$_{PAH}$ express lower levels of ITSN-1s compared with controls and the GrB-EH$_{ITSN}$ cleavage product. Moreover, GrB immunoreactivity is associated with PLs in PAH lungs. The concurrent expression of the two cleav-age products results in a high p38/Erk1/2^{MAPK} activity ratio, which is critical for EC proliferation. Our findings identify a novel GrB-EH$_{ITSN}$-dependent pathogenic p38^{MAPK}/Elk-1 signaling pathway involved in the poorly understood process of PL formation in severe PAH.

PAH[2] is a disease of the small pulmonary arteries (PAs) characterized by vascular proliferation, remodeling, and the progressive formation of hallmark PLs that increase pulmonary vascular resistance, ultimately leading to right ventricular failure and death (1). Enhanced proliferation and decreased apoptosis in ECs, pulmonary artery smooth muscle cells, and fibroblasts are central to the pathogenesis of PAH. EC growth and the emergence of phenotypically altered, proliferative ECs in severe PAH are a consequence of initial EC dysfunction, apoptotic death, and subsequent selection of apoptosis-resistant, proliferative vascular cells (2, 3). Human studies of PLs are limited; whether or not they are the cause or the effect of hypertension is not understood. The cellular and molecular mechanisms responsible for PL development are not known. We recently reported that human lung EC dysfunction in a proinflammatory setting is associated with down-regulation of ITSN-1s, a general endocytic protein essential for EC survival, as well as up-regulation of antiapoptotic Bcl-X$_L$ and survivin

---

1 To whom correspondence should be addressed: Depts. of Pharmacology and Pulmonary and Critical Care Medicine, Rush University Medical Center, 1735 W. Harrison St., 1535 JS, Chicago, IL 60612. Tel.: 312-563-2437; Fax: 312-942-0339; E-mail: sanda_predescu@rush.edu.

2 The abbreviations used are: PAH, pulmonary arterial hypertension; Ab, antibody; EC, endothelial cell; FD, failed donor; GrB, granzyme B; IHC, immunohistochemistry; ITSN-1s, intersectin-1 short; MCT, monocrotaline; PA, pulmonary artery; PL, plexiform lesion; SRE, serum response element; SH3, Src homology 3; PAEC, pulmonary artery endothelial cell; EH, Eps15 homology; MTT, 3-(4,5-dimethylthiazol-2-yl)-2,5-diphenyltetrazolium bromide; pAb, polyclonal antibody; Ctrl, control.

(4), suggesting that inflammation may not only cause EC dysfunction but also qualitatively change their phenotype. Bcl-X_L is increased in animal models of PAH as well as in PAECs isolated from EC_{PAH} (5–7). Significantly, Bcl-X_L overexpression renders resistance to GrB-induced apoptosis (8). Evidence indicates that inflammation associated with human PAH attracts $CD8^+$ T-cells, which release the cytotoxic protease GrB (9–12). $CD8^+$ T-cells are significantly increased in the lungs of rats with monocrotaline (MCT)-induced PAH at 3 weeks, suggesting a particular phenomenon related to PAH evolution (13). GrB is implicated in the pathogenesis of several chronic inflammatory diseases mainly because of its well established proapoptotic role (14). Non-cytotoxic roles of GrB, non-apoptotic pathways, and gain of function of the GrB cleavage fragments, still controversial observations, were also reported recently (15).

ITSN-1s is a putative substrate for GrB with a cleavage site at $IDQD^{271}GK$ (16). ITSN-1s is a multimodular protein comprising two Eps15 homology (EH) domains, a central coiled coil domain, and five consecutive Src homology 3 (SH3A–SH3E) domains (17). This multimodular structure implicates ITSN-1s in multiple protein-protein interactions essential for efficient vesicular trafficking, cytoskeletal rearrangements, regulation of cell signaling pathways, survival, and tumorigenesis (18–23). Thus, ITSN-1s cleavage by GrB, resulting in decreased expression of full-length protein and two cleavage products, may impact essential biological processes and pulmonary EC function. *In vivo* knockdown of ITSN-1s triggers apoptosis of mouse lung ECs in a process that involves down-regulation of MEK/Erk1/2^{MAPK} survival signaling (22). After only 7 days of ITSN-1s knockdown, the remaining ECs showed phenotypic changes toward increased proliferation and apoptosis resistance, leading to repair and remodeling of the injured lungs; apparently, a signaling switch downstream of Alk5, a broadly expressed TGFβ type 1 receptor (24), from the canonical Smad2/3 to Ras/Erk1/2^{MAPK} signaling protected ECs from impending apoptosis caused by ITSN-1s deficiency and triggered changes in EC phenotype toward enhanced proliferation (22). It has been reported that both TGFβ and bone morphogenetic protein activate Smad-independent MAPK signaling pathways, including Erk1/2 and p38 (25). Phosphorylation of Erk1/2 and/or p38 is increased in experimental models of PAH (26). Although heterozygous mutations in the type II receptor for bone morphogenetic protein underlie the majority of the inherited and familial forms of PAH and may explain the abnormal TGFβ and bone morphogenetic protein signaling, the underlying mechanisms of Erk1/2/p38 activation are not yet understood for a significant group of PAH subjects, and additional factors have been suspected. Thus, we hypothesized that a decrease in full-length ITSN-1s expression due to GrB cleavage during inflammatory reactions associated with PAH and the opposing effects of GrB/ITSN-1s cleavage products on Erk1/2/p38^{MAPK} activation unbalance the activity ratio of p38 to Erk1/2 signaling, leading to EC proliferation and selection of a proliferative/plexiform phenotype.

EXPERIMENTAL PROCEDURES

Materials—Human PAECs were obtained from Lonza (Walkersville, Inc., MD). PAECs isolated from idiopathic PAH subjects were kindly provided by Lerner Research Institute, Cleveland Clinic and Dr. Roberto Machado (University of Illinois at Chicago). X-tremeGENE 9 DNA transfection reagent and *In Situ* Cell Proliferation kit (BrdU assay) were from Roche Applied Science. ProLong Antifade kit with DAPI was from Molecular Probes (Eugene, OR). MicroBCA (bicinchoninic acid) protein assay reagent, BSA, ECL Western blotting substrate, NE-PER Nuclear and Cytoplasmic Extraction kit, and LightShift Chemiluminescent EMSA kit were from Pierce. Nitrocellulose membranes were from Bio-Rad. 3-(4,5-Dimethylthiazol-2-yl)-2,5-diphenyltetrazolium bromide (MTT) Cell Proliferation Assay kit was from ATCC (Manassas, VA). ChIP-IT Express kit and Elk-1 activation kit were from Active Motif (Carlsbad, CA). SB203580 was purchased from Promega (Madison, WI). HyBlot CL autoradiography films were from Denville Scientific Inc. (South Plainfield, NJ). Glutathione-Sepharose 4 Fast Flow beads were from GE Healthcare. Recombinant heat shock protein (Hsp) 90 was purchased from Enzo Life Sciences (Farmingdale, NY). LPS and GrB were from Sigma-Aldrich, and MCT was from Oakwood Products, Inc. (West Colombia, SC).

Specific antibodies (Abs) were obtained from the following sources. Erk1/2 pAb, phospho-Erk1/2 mAb, p38 pAb, phospho-p38 mAb, JNK pAb, phospho-JNK pAb, PI3K pAb, phospho-PI3K pAb, Akt pAb, phospho-Akt pAb, c-Fos pAb, and myc pAb were obtained from Cell Signaling Technology (Beverly, MA). ITSN-1 Ab against the N terminus of ITSN-1 was generated as described (27). ITSN-1 pAb used for immunohistochemistry (IHC) was from Sigma-Aldrich. Elk-1 pAb, GrB mAb, and PECAM-1 pAb were from Santa Cruz Biotechnology (Santa Cruz, CA). Alexa Fluor fluorophore-conjugated anti-mouse IgG and anti-rabbit IgG were purchased from Molecular Probes. HRP-conjugated reporters were from Cappel, Organon Teknika (Durham, NC).

Cell Culture—Control and transfected ECs were grown in EBM-2 and medium 199 supplemented with 20% FCS as described previously (19). EC_{PAH} were grown as described (28).

EH_{ITSN} (Amino Acids 1–271), Full-length ITSN-1s Constructs, and Transfection Procedure—The cDNA encoding EH domain (amino acids 1–271) of human ITSN-1s cDNA fragment (813 bp) was generated by PCR amplification from ITSN-1L cDNA (a gift from Suzana la Luna, Center for Genomic Regulation, Pompeu Fabra University and Centro de Investigacion Biomedica en Red de Enfermedades Raras, Barcelona, Spain) with High Fidelity PCR enzyme (New England Biolabs) using the following primer pair: ITSN1_F269-EcoRI (5′-AGTA<u>GAATTC</u>GCCACCATGGCACAGTTTCCAACACC-3′) and ITSN1_R1082-XbaI (5′-CGTA<u>TCTAGA</u>ATCTTGATCAATGTCAGAAAGATTCC-3′). The PCR products of ITSN-1s (~813 bp) were digested with restriction enzymes (restriction sites are underlined) EcoRI and XbaI (New England Biolabs), purified (Qiagen purification kit), then cloned into expression vector (N-myc) CS-Z3999-M43 (GeneCopoeia) at EcoRI-XbaI sites, and transformed into *Escherichia*

coli strain Top10 (Invitrogen). The plasmid DNA was extracted from several selected growing clones, and the presence of the ITSN-1s insert was verified with PCR, restriction enzyme (EcoRI and XbaI) digestion, and sequencing confirmation of the integrity of the entire cDNA fragment of ITSN-1s (813 bp of EH domain, which is a 100% match with GenBank™ accession number AF114487) in-frame inside the vector in one of the clones. A similar approach was used for full-length human ITSN-1s cDNA fragment using the following primer pair: ITSN1s_F269-BstBI (5′-AGTA**TTCGAA**CCATGGCTCAGT-TTCCAACACCTT-3′) and ITSN1s_R3929-NheI (5′-CGTA**G-CTAGC**TTGCTGGCTTGGGTCCATGTCTG-3′). All transfections were performed using a 3:1 ratio of X-tremeGENE 9 DNA transfection reagent (μl) to DNA (μg) according to the manufacturer's protocol.

Expression and Purification of GST Fusion Proteins—ITSN(1–440)-GST was generated by subcloning the PCR-amplified ITSN-1, residues 1–440, into the pGEX-4T-1 vector (GE Healthcare). The following primer pair was used: ITSN1_F269 (5′-CCCG**GAATTC**ATGGCTCAGTTTCCAACACCTT-3′) and ITSN1_R1588 (5′-CGAT**GCGGCCGC**TATTCCCGTT-TTGCAGCCTCTCG-3′).

For mutagenesis, aspartic acid (D) at position 271 of EH domain of human ITSN1 was mutated to glutamic acid (E). PCR primers bearing the mutated sequence, ITSN_D271E_R (5′-CCTCTGCTGTAAGTTTACC**CTC**TTGATCAATGTCA-GAAAG-3′) and ITSN1_D271E_F (5′-CTTTCTGACATTGA-TCAA*GA*GGGTAAACTTACAGCAGAGG-3′), were used, and the amplified PCR products with the mutation D271E (using High Fidelity PCR enzyme with pGEX_ITSN1s_EH-1–440 wild type as template) were digested with EcoRI and NotI and subcloned into the EcoRI-NotI sites of pGEX-4T-1 vector. After the resulting cDNA vectors were verified by DNA sequencing to ensure sequence integrity, they were transformed into *E. coli* BL-21(DE3) pLysS (Invitrogen). The GST fusion proteins were then purified as described previously (29).

MCT-induced PAH in the Mouse—PAH was induced in mice as described (30). MCT was dissolved in 0.1 M HCl, neutralized with 0.1 M NaOH to pH 7.4, and sterilized through a 0.22-μm filter. CD1 mice (3 months; 25 g) were injected subcutaneously with MCT at 30 mg/100 g of body weight once a week for 8 weeks. Six mice (three males and three females) were used per experiment. All animals were sacrificed 8 days after the last MCT administration. Lungs (free of blood) were excised and used to prepare lung lysates as described previously (31). Repeated MCT administration and prolonged treatment compensate for strain- and species-specific differences between hepatic cytochrome P450 enzyme required for MCT processing to active MCT pyrrole and allow consistent, reproducible induction of PAH in mice (30, 32, 33). MCT injections were given without anesthesia. All animal studies were performed in accordance with the guidelines of the Rush University Institutional Animal Care and Use Committee. All surgeries were performed under anesthesia using intraperitoneal delivery of ketamine hydrochloride/xylazine hydrochloride solution (1 ml/kg of body weight) (Sigma).

Protein Extraction and Western Blotting—ECs grown on Petri dishes were collected and solubilized in lysis buffer (20 mM

Tris-HCl, pH 7.4, 150 mM NaCl, 0.3% SDS, 1% (w/v) Triton X-100, 1 mM Na_3VO_4, 1 mM PMSF, and protease and phosphatase inhibitors) for 1 h at room temperature under gentle agitation. For detection of phosphorylated protein, cells were lysed in kinase buffer (20 mM Tris-HCl, pH 7.4, 150 mM NaCl, 0.3% SDS, 1% (w/v) Triton X-100, 1 mM Na_3VO_4, 1 mM PMSF, and protease and phosphatase inhibitors). The resulting lysate was clarified by centrifugation in a Beckman Optima Max-XP ultracentrifuge with a TLA-55 rotor at 45,000 rpm for 45 min at 4 °C. Protein concentration was determined using the BCA method with a BSA standard. Protein samples normalized for total protein were subjected to SDS-PAGE and transferred to nitrocellulose membranes. Strips of nitrocellulose membranes were incubated with the primary and reporter Abs and processed as described (27). The reaction was visualized using ECL and HyBlot CL films. Representative HyBlot CL films were subjected to densitometry using NIH ImageJ software.

In Vitro and In Vivo GrB Cleavage Assays—For *in vitro* cleavage, purified Hsp90, ITSN(1–440)-GST, or ITSN(1–440)-GST (D271E) protein at 70 μg/ml was incubated at 37 °C with recombinant human GrB (500 nM) in GrB activity buffer (50 mM Na-HEPES, pH 8.0, 100 nM NaCl, and 0.01% Tween 20) for 2h, then mixed with sample loading buffer, and resolved by SDS-PAGE followed by Coomassie staining (34). For the cleavage *in vivo*, CD31 mice were treated with 90 μg of LPS/mouse for 1, 4, and 6 h, and lung lysates were subjected to SDS-PAGE followed by electrotransfer and immunoblotting with Abs against ITSN-1. The presence of GrB in the mouse lung lysates was detected by Western blotting with GrB Ab. Lung tissue of rats with MCT-induced PAH was kindly provided by Dr. Jiwang Chen (University of Illinois at Chicago) and analyzed as above.

MTT Assay—Cell viability was examined with the MTT cell proliferation kit in accordance with the manufacturer's instructions. Briefly, triplicate aliquots of cells (10^6 cells suspended in 100 μl of complete EC medium) were seeded onto a 96-well plate, and serial dilutions were prepared in EC medium. Cells were cultured for 48 h followed by addition of 10 μl of MTT reagent to each sample. After a 5-h incubation, 100 μl of detergent was added to each well, and the plate was covered and kept in the dark at room temperature overnight. Absorbance was measured at 595 nm in a microtiter plate reader on the following day. Parallel triplicate experiments using non-treated ECs were performed, cells were counted using a hemocytometer, and a growth curve was generated to relate the A_{570} values to the cell number per well.

Cell Proliferation Assay—Cell proliferation was determined using the *In Situ* Cell Proliferation kit. Cells were grown on coverslips for 48 h and then transfected with myc-GrB-EH$_{ITSN}$ as above. BrdU incorporation was performed according to the manufacturer's instructions. Briefly, cells were incubated in culture medium containing 10 μM BrdU labeling solution for 6 h at 37 °C. Cells were then washed with PBS and fixed, and the DNA was denatured followed by incubation with BrdU-FLUOS Ab (45 min at 37 °C) in a humid chamber. Cells were again washed with PBS, and the coverslips were mounted using the ProLong Antifade kit. The BrdU-positive cells were counted on high power field images, and data were expressed as the number of BrdU-positive cells per 50 high power fields.

Elk-1 Transcription Factor Assay—Nuclear extracts of control and transfected cells were prepared using the NE-PER Nuclear and Cytoplasmic Extraction kit according to the manufacturer's protocol. The nuclear extracts were then analyzed by ELISA (TransAM kit with colorimetric readout quantifiable by spectrophotometry) in a 96-well plate containing the immobilized Elk-1 consensus site oligonucleotide. Activated Elk-1 was detected via an Ab against phosphorylated Elk-1 followed by an HRP-conjugated reporter Ab. The plates were read at 450 nm using a Dynex plate reader. Data from triplicate wells in three different experiments were expressed as a mean ± S.E.

Immunofluorescence Microscopy—ECs grown on plastic coverslips were washed with cold PBS (three times for 5 min), fixed (methanol for 7 min at −20 °C), quenched (1% BSA in PBS for 1 h at room temperature), and incubated with appropriate primary Ab diluted in 0.1% BSA in PBS for 1 h. After washing with 0.1% BSA in PBS (three times for 10 min), the cells were incubated for 1 h with appropriate reporter Abs, washed again as above, then mounted on glass slides using ProLong Antifade reagent, examined, and photographed in a Zeiss AxioImager M1 microscope equipped with a digital camera.

IHC on paraffin-embedded human lung tissue sections was performed using ITSN-1 Ab (C-terminal epitope; the only commercially available Ab efficient in IHC); the generally accepted EC marker, CD31; GrB Ab; and phospho-p38 Ab. All were followed by the appropriate Alexa Fluor 488- or Alexa Fluor 594-conjugated reporter as described (22). CD31 and GrB Abs were used at 1:200 dilution in 0.1% BSA in PBS, whereas ITSN-1 and phospho-p38 Abs were used at 1:100 dilution.

Gel Shift Assay—The gel shift assay was carried out with the Light Shift chemiluminescent EMSA kit according to the manufacturer's instructions. Briefly, 20 fmol of biotin-labeled double-stranded probe (Sigma-Aldrich) containing the Elk-1 binding site (underlined) in the c-*fos* serum response element (SRE; 5′-TCGACAGGATGTCCATATTAGGACATCTGCGTCAGCTCGA-3′) was incubated with 10 µg of nuclear extract in a 20-µl binding reaction containing 2 µl of binding buffer (100 mM Tris, 500 mM KCl, and 10 mM DTT, pH 7.5), 1 µg of poly (dI-dC), 2.5% glycerol, 5 mM $MgCl_2$, and 0.05% Nonidet P-40 for 20 min at room temperature. For competition experiments, a 100-fold excess of unlabeled probe was added to the reaction. The DNA·protein complexes were resolved on a 5% nondenaturing polyacrylamide gel, transferred to a positive nylon membrane (Fischer Scientific), cross-linked in a 1800 UV Stratalinker. Then the membranes were incubated with streptavidin-in-HRP followed by chemiluminescent substrate before being exposed to HyBlot CL films to visualize the DNA·protein complexes. 2 µg of anti-Sap-1a and anti-Elk-1 Abs was added for the supershift assay.

ChIP Assay—The ChIP was performed using a ChIP-IT Express kit according to the manufacturer's instructions. Briefly, control and myc-GrB-EH$_{ITSN}$-transfected ECs (1.5 × 10^7 cells; 48 h post-transfection) were fixed in 1% formaldehyde (10 min at room temperature). The cell lysates were centrifuged to pellet the nuclei at 5000 rpm for 10 min at 4 °C. DNA was sheared into 200–800-bp fragments using a Branson sonicator 450 (five pulses at 25% power; each pulse consisted of 20-s sonication followed by a 1-min rest). After centrifugation, an aliquot (10 µl) of the sheared DNA was saved as the input sample for PCR. Sheared chromatin (10 µg) was then incubated with 2 µg of rabbit IgG or Elk-1 Ab and 25 µl of protein G magnetic beads overnight at 4 °C. After reversal of cross-linking and protein digestion with protease K, precipitated DNA and input DNA were purified using the QIAquick PCR purification kit (Qiagen) and subjected to real time PCR amplification with SYBR Green dye on an Applied Biosystems (Carlsbad, CA) real time thermocycler. c-*fos* promoter fragment containing the Elk-1 binding site was amplified using forward primer 5′-TCC-GTACAAGGGTAAAAAGG-3′ and reverse primer 5′-CTAA-TCTCGTGAGCATTTCG-3′.

RT-PCR—ECs were lysed using the Qiagen QIAShredder homogenizer, and total RNA was isolated using the Qiagen RNeasy Mini RNA isolation kit according to the manufacturer's instructions. The cDNA was synthesized from 2 µg of RNA using a High-Capacity cDNA Reverse Transcription kit (Applied Biosystems) according to the manufacturer's protocol. Amplification was carried out using the following primer pair for human ITSN-1s: forward, 5′-CAGGCTTGAAAGTC-CTCAAAG-3′; reverse, 5′-GGTGATCATGCTGGAAGTCA-3′. An equal volume of cDNA was amplified with Go Taq Green Master Mix (Promega, Madison, WI) in a C1000 thermal cycler (Bio-Rad). The reactions consisted of a 3-min denaturation step at 95 °C, 32 cycles of denaturation at 95 °C for 30 s followed by annealing for 30 s at 60 °C, and extension for 30 s at 72 °C followed by 5 min at 72 °C. The PCR products were resolved on a 1.2% agarose gel and visualized using ethidium bromide staining. Relative amounts of RNA were assessed by comparing the amount of PCR product for ITSN-1s with the PCR product for cyclophilin.

Human PAH Biospecimens—EC$_{PAH}$ were derived from the lungs of three patients with idiopathic PAH at the Cleveland Clinic Foundation (28). IHC studies were performed on 12 PAH and one failed donor lung tissue (FD$_1$-Ctrl) biospecimens (paraffin-embedded lung tissue) identified from autopsy files at Rush University and the University of Chicago. Frozen PAH lung tissue and FD$_2$-Ctrl (kindly provided by Dr. Anna Ryan-Hemnes, Allergy, Pulmonary, and Critical Care Medicine, Vanderbilt University) were used for biochemical investigations. The studies were approved by the Rush Human Subject Committee. Informed consent from the patients was obtained in all cases. Clinical diagnosis, underlying conditions, and other pertinent clinical and laboratory data were reviewed. Lung histological sections were analyzed in each case.

Statistical Analysis—All data are expressed as mean ± S.E. (error bars). Statistical analysis was performed using Student's *t* test and analysis of variance for comparison of variance between different groups. A value of $p < 0.05$ was considered significant.

RESULTS

GrB Cleaves ITSN-1s in Vitro and in Vivo—The identification in ITSN-1s of a potential cleavage site (IDQD^{271}GK) for GrB prompted us to confirm this cleavage *in vitro* and *in vivo*. For *in vitro* assessment, we generated a truncated human ITSN-1s, tagged with GST (ITSN(1–440)-GST; molecular mass, 78 kDa) as described (29), that contained the GrB cleavage site.
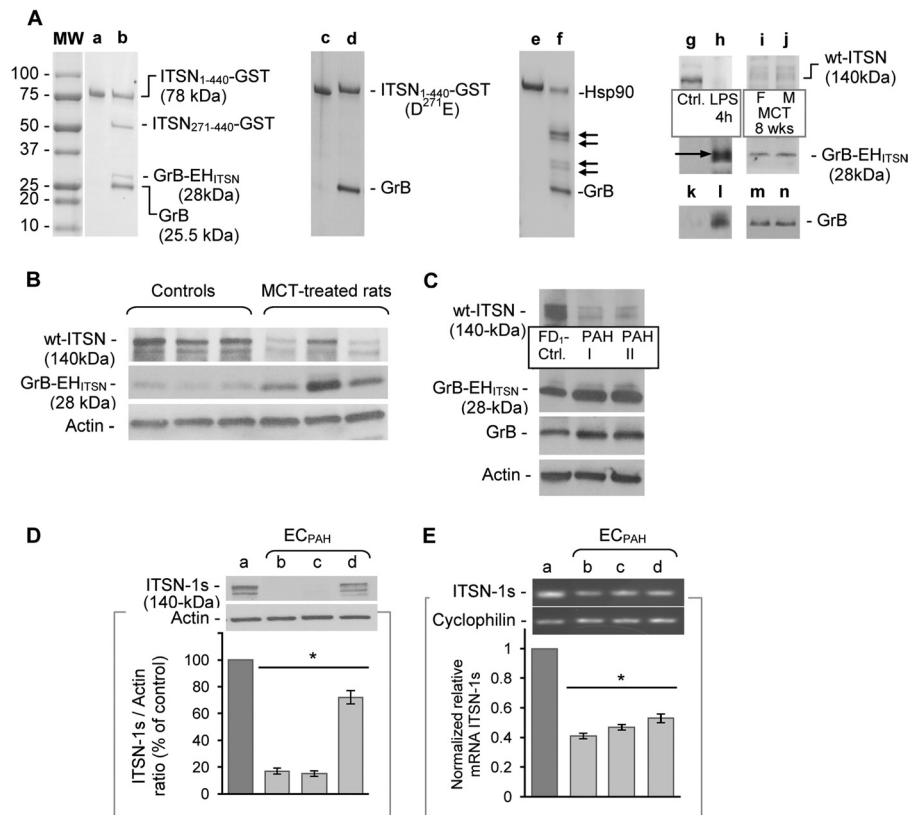
FIGURE 1. **GrB cleaves ITSN *in vitro* and *in vivo*.** *A, in vitro* cleavage of affinity-purified ITSN(1–440)-GST (*lane a*) by 500 nM hGrB followed by SDS-PAGE/Coomassie staining results in GrB-EH$_{ITSN}$ and a 50-kDa C-terminal fragment, ITSN(271–440)-GST (*lane b*). The mutant ITSN(1–440)-GST (D271E) is not cleaved by the same amount of GrB (*lanes c and d*). Hsp90 was used as control (*lanes e and f*); *arrows* in *lane f* indicate the GrB cleavage products. Western blot of lung lysates of LPS-treated mice (4-h LPS exposure) with ITSN Ab (N-terminal epitope) shows loss of full-length ITSN-1s (*lane h versus lane g*) and the appearance of GrB-EH$_{ITSN}$ cleavage product (*arrow*). GrB is detected by Western blot in mouse lung lysates at 4 h after 90 μg of LPS/mouse (*lane l*). No GrB immunoreactivity was detected in untreated mice (*lane k*). PAH was induced in CD1 mice (females (*F*) in *lane i* and males (*M*) in *lane j*). Western blot revealed decreased ITSN-1 expression and presence of GrB-EH$_{ITSN}$ cleavage product (*lanes i and j versus lane g*) as well as GrB expression (*lanes m and n*). *n* = 3. The control (*lane g*) shows the level of ITSN-1s in a 3-month-old CD1 mouse. It is a suitable control for both LPS- and MCT-treated mice because studies indicated that 3–6-month-old CD1 mice show similar levels of ITSN. Sequence alignment shows a conserved GrB cleavage site in rodents and humans (blast.ncbi.nlm.nih.gov). *B*, male Sprague-Dawley rats (200–250 g) were injected with one dose of MCT (60 mg/kg intraperitoneally). Four weeks after treatment, the lungs were perfused with PBS, harvested, and used to prepare tissue lysates that were subjected to Western blot analyses using ITSN-1 Ab. Actin was used as a loading control. *C*, human lung lysates (70 μg of protein) of FD$_1$-Ctrl and PAH tissue (two different locations: PAH I and PAH II) were subjected to SDS-PAGE and electrotransfer followed by Western blot using ITSN-1 and GrB Abs. *D*, decrease of full-term ITSN-1s was also detected in EC$_{PAH}$ lysates (*lanes b, c*, and *d*) by reference to a representative EC$_{Ctrl}$ (*lane a*; the studies were performed on three different batches/donors and Lonza EC$_{Ctrl}$ with similar results). Data are representative for three different EC$_{PAH}$ preparations: EC$_{PAH}$-B397 (*lane b*), EC$_{PAH}$-CC-005 (*lane c*), and EC$_{PAH}$-CC016 (*lane d*). ITSN-1s down-regulation quantified by densitometry was different among the three EC lines used. *E*, RT-PCR and densitometry of ITSN-1s mRNA levels in EC$_{PAH}$ (*lanes b, c*, and *d*) by reference to EC$_{Ctrl}$ (*lane a*). Data are representative for three independent experiments applied on EC$_{Ctrl}$ and three different EC$_{PAH}$ lines: B397 (*lane b*), CC-005 (*lane c*), and CC016 (*lane d*). Results are expressed as mean ± S.E. (*error bars*). *, $p < 0.001$ *versus* control. All data are representative of three independent experiments. LPS and MCT treatments were applied to at least three mice per experimental condition.

Affinity-purified ITSN(1–440)-GST (Fig. 1*A*, *lane a*) was then exposed to recombinant human GrB. Proteolysis of ITSN-1s by GrB generated two cleavage products with M_r 28,000 and 50,000, consistent with the predicted cleavage site (Fig. 1*A*, *lane b*). Site-directed mutagenesis (aspartic acid (Asp^{271}) mutated to glutamic acid) generated an ITSN(1–440) protein resistant to GrB cleavage and confirmed the specificity of the cleavage (Fig. 1*A*, *lane d versus lane c*). Recombinant Hsp90, a known GrB substrate (34), was used as a positive control (Fig. 1*A*, *lane f* (*arrows*) *versus lane e*). To address the susceptibility of ITSN-1s to native GrB and to evaluate the *in vivo* cleavage, we exposed mice to LPS for 1, 4, and 6 h. The bacterial endotoxin induces a strong immune response in mice, including an increase in GrB and perforin expression (35, 36). Western blot using an Ab against the N terminus of ITSN-1s (27) applied on LPS-treated mouse lung lysates 4 h post-LPS exposure revealed the loss of full-length ITSN-1s protein expression and presence of the

28-kDa N-terminal fragment, GrB-EH$_{ITSN}$ (Fig. 1*A*, *lane h versus lane g*). This is consistent with cleavage of ITSN-1s at the predicted site by GrB produced by the CD8$^+$ T-lymphocytes in LPS-treated mouse lungs. Moreover, Western blot of LPS-treated mouse lung lysates with GrB Ab indicated the presence of GrB as early as 1 h post-LPS treatment (not shown) and significantly higher levels at 4 h (Fig. 1*A*, *lane l*). Cleavage of ITSN-1s by GrB was minimal at 1 h post-LPS treatment, whereas at 6 h post-LPS exposure, the levels of GrB and the extent of ITSN-1s cleavage were similar to those at the 4-h time point (not shown). No GrB immunoreactivity was detected in untreated mice (Fig. 1*A*, *lane k*). To further confirm the *in vivo* cleavage of ITSN-1s by GrB and its connection to PAH, we applied similar analyses on lung tissue of PAH animal models. We studied the MCT-induced PAH mouse model that displays marked pulmonary inflammation, hypertrophy of PAs with occlusion of precapillary vessels, and 2.5-fold elevation in right

TABLE 1

Characteristics of autopsied patients

F, female; M, male; NA, not applicable; RV, right ventricle; GI, gastrointestinal.

Autopsy no.	Etiology	Race	Sex	Age	Duration of disease	Cause of death	Pulmonary arterial pressure	Cardiac output	PLs
							mm Hg	*liter/min*	
1	Idiopathic	Hispanic	F	47	7 years	RV failure	NA	NA	12
2	Idiopathic	African-American	M	51	3.5 years	RV failure	53	4	6
3	Idiopathic	Caucasian	F	27	2 months	RV failure	NA	NA	5
4	Idiopathic	Hispanic	F	29	7 years	RV failure	52	4.42	8
5	Idiopathic	African-American	F	53	23 years	Cancer	63	6.76	1
6	Idiopathic	Caucasian	F	71	18 years	RV failure	59	3.8	2
7	Idiopathic	Caucasian	F	76	6 years	RV failure	46	4.6	5
8	Idiopathic	Caucasian	F	48	7 years	RV failure	59	3.05	7
9	Idiopathic	Caucasian	F	56	6 years	Upper GI bleed	54	3.3	2
10	Idiopathic/familial?	Caucasian	M	42	<7 years	RV failure	69	5.07	3
11	Lupus	Filipino	F	45	15 years	RV failure	45	0.33	3
12	Chronic pulmonary embolism	African-American	F	64	4 years	RV failure	82	4.73	3

ventricular pressure (30). MCT was administered to mice by subcutaneous injections of 30 mg of MCT/100 g of body weight for 8 weeks as described previously (30). At the end of the treatment, the lungs were collected, and tissue lysates were prepared and further subjected to immunoblotting analyses. Decreases in full-length ITSN-1s and the GrB-EH$_{ITSN}$ cleavage product were easily detected (Fig. 1*A, lanes i* and *j versus lane g*), further confirming the *in vivo* cleavage of ITSN-1s by GrB in the lungs of the MCT-treated mouse. GrB immunoreactivity was also detected in MCT-treated mouse lung lysates (Fig. 1*A, lanes m* and *n*). Similar results were obtained when lung tissue lysates of an MCT rat model of PAH were analyzed (Fig. 1*B*). All MCT-treated rat lung lysates also show immunoreactivity for the GrB-EH$_{ITSN}$ fragment. Actin was used as a loading control. Given the high endothelial content of lung tissue (37, 38), these findings are highly significant for ECs of the lung. Thus, we concluded that ITSN-1s is a substrate of GrB, and its proteolytic cleavage is associated with the PAH condition in animal models.

Lung ECs of PAH Subjects Express Low Levels of Full-length ITSN-1s—Next, expression of ITSN-1s was investigated in explanted human lung tissue of a 32-year-old white female transplanted for severe PAH; tissue was sampled from two different locations (PAH I and PAH II). A marked decrease in ITSN-1s protein and significant immunoreactivity for the GrB-EH$_{ITSN}$ were easily detected by comparison with FD$_1$-Ctrl (Fig. 1*C*). Weaker immunoreactivity for the GrB-EH$_{ITSN}$ fragment was also detected in the FD$_1$-Ctrl lysates. Given the previous reports of inflammatory markers, including GrB and perforin, in bronchoalveolar lavage and alveolar lymphocytes during acute and chronic lung rejection (39, 40), we investigated GrB expression in both FD$_1$-Ctrl and PAH lung tissue lysates and found that both were immunoreactive to GrB (Fig. 1*C*). However, GrB immunoreactivity in FD$_1$-Ctrl lysates is 60% lower than under PAH conditions as estimated by densitometry. Thus, GrB produced during lung rejection may account for the GrB-EH$_{ITSN}$ presence in the FD$_1$-Ctrl lysates. Actin was used as a loading control. The observations strongly suggest that the 28-kDa fragment is the result of GrB cleavage of ITSN-1s.

We also evaluated the expression of ITSN-1s protein in EC$_{PAH}$. Commercially available human normal PAECs were used as controls (EC$_{Ctrl}$). ITSN-1s down-regulation is obvious

in all EC$_{PAH}$ by reference to EC$_{Ctrl}$ (Fig. 1*D*); however, the degree of ITSN-1s down-regulation among EC$_{PAH}$ ranged from 30 to 80%. A 28-kDa protein band that was immunoreactive to ITSN-1 Ab was also detected only when longer ECL exposures of the nitrocellulose membranes were applied (not shown). Given the lack of CD8$^+$ T-cells and GrB in cultured ECs, we also evaluated by RT-PCR the levels of ITSN-1s mRNA in EC$_{PAH}$ by reference to EC$_{Ctrl}$. EC$_{PAH}$ show on average about 50% lower levels of mRNA (Fig. 1*E*). Real time PCR as described (4, 28) confirmed the extent of ITSN-1s mRNA down-regulation in EC$_{PAH}$ compared with EC$_{Ctrl}$ (not shown). These results strongly indicate a stable EC phenotype and a possible regulation of ITSN-1s and EH$_{ITSN}$ expression in late stage PAH at mRNA levels and by alternative mRNA splicing, a process highly characteristic to ITSNs (41). Altogether, the findings demonstrate that ITSN-1s is down-regulated in lung EC$_{PAH}$.

The level of ITSN-1s in lung ECs of human PAH subjects was further evaluated by ITSN-1s/CD31 IHC on paraffin-embedded tissue sections. We analyzed 12 PAH cases (Table 1). Representative histology (H&E) of lung tissue from PAH specimens showed PA remodeling, intimal fibrosis, and complex PLs (Fig. 2, *a–k*). Control lung sections showed no evidence of PA remodeling or interstitial inflammation (Fig. 2*l*). For IHC studies, we used an ITSN-1 Ab against a C-terminal epitope (the only commercially available Ab efficient for staining of paraffin embedded-tissue) that does not recognize the N-terminal GrB-EH$_{ITSN}$. We focused on highly rich EC areas (PL-like) that show hypercellularity and strong CD31 (accepted EC marker) staining (Fig. 3, *A* and *B*). A complex lesion with focal proliferation of several endothelial channels and partial destruction of the arterial wall (Fig. 3*A, panel a1*) shows low ITSN-1s immunoreactivity (*panel a2*) and limited CD31/ITSN-1s co-localization (Fig. 3*A, panel a4, arrow*). The thin walled lymphatic (Fig. 3*A, panels a1* and *a4* (*asterisk*)) in close PL proximity shows barely detectable ITSN-1s immunoreactivity as well. DAPI was used for nuclear staining (Fig. 3*A, panel a3*). Patchy ITSN-1s staining, most likely associated with airway epithelial cells (Fig. 3, *panel a4, arrowheads*), was commonly detected. Clusters of proliferative ECs surrounded by concentric intimal thickening (Fig. 3*B, panels b1* (*circled area*) and *b2*) and lacking ITSN-1s (Fig. 3*B, panels b2* and *b2.1*) are seen in the lumen of a small PA. Lack of ITSN-1s is characteristic not only of ECs but also of
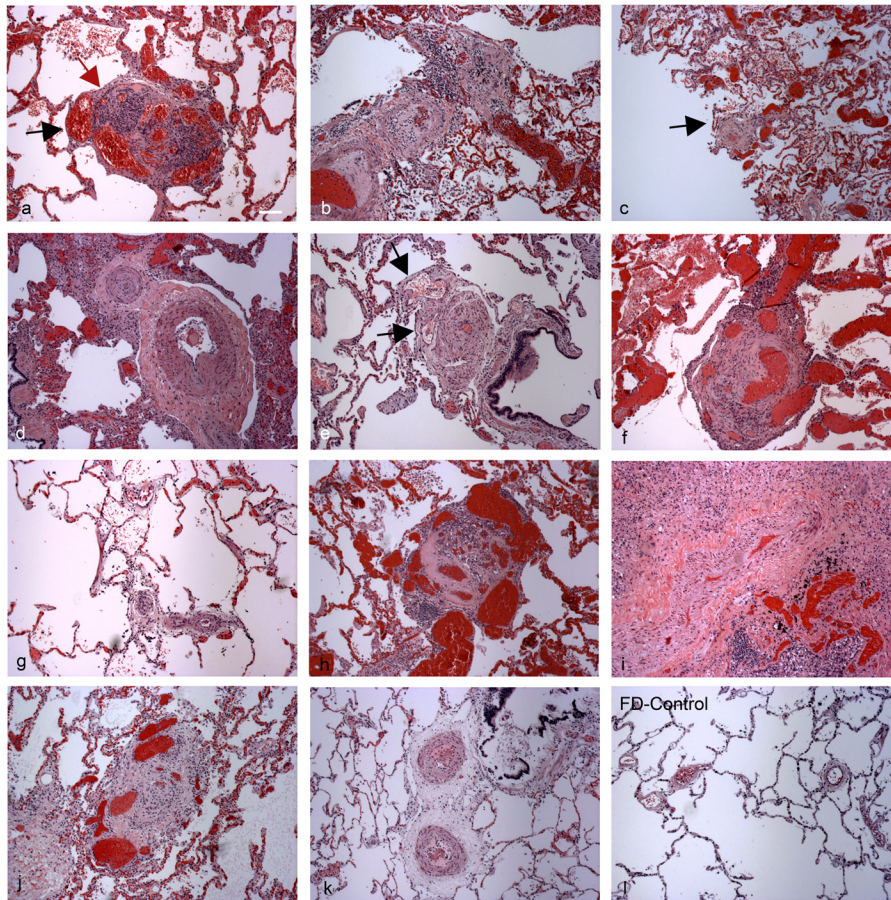
FIGURE 2. **Pathological findings in PAH patients.** PA vasculopathy with PL (*brown arrow*) and associated angiomatoid dilation (*black arrow*) (*a*), eccentric intimal fibrosis in lumen of artery with near occlusion of smaller adjacent branch (*b*), muscularization of arteriole without intimal fibrosis (*c*, *arrow*), medial hypertrophy and concentric medial fibrosis (*d*), media hypertrophy and cellular occlusion of lumen of the artery with adjacent angiomatoid dilation of vessel (*arrows*) likely with an associated PL in another plane (*e*), PL with associated angiomatoid dilation (*f*), muscularization of arteriole (*g*), PL and associated angiomatoid dilation (*h*), intimal fibrosis and medial proliferation of collapsed PA (*i*), concentric intimal fibrosis and medial hypertrophy and adjacent dilation lesion (*j*), intimal fibrosis and medial hypertrophy (*k*), and normal control (*l*). *Scale bar*, 100 μm (*a–l*).

other intimal cells (Fig. 3*B*, panel b2). ITSN-1s staining was also decreased in ECs lining the small blood vessels not yet detectably affected by remodeling in PAH specimens (Fig. 3*D*, inset) compared with control (Fig. 3*C*, inset). Note also the scarce ITSN-1s staining in all other resident lung cells of the PAH specimen compared with the FD$_2$-Ctrl (Fig. 3*D*). Weak ITSN-1s staining using an ITSN-1s Ab supposed to recognize not only the full-length protein but also the C-terminal GrB cleavage fragment strongly supports the concept that, in late stage PAH, ITSN-1s expression may also be regulated at the mRNA level as also suggested by the EC$_{PAH}$ phenotype. Altogether, these observations provide undeniable evidence that ITSN-1s deficiency is associated with the PAH condition in human.

GrB Immunoreactivity in the Microenvironment of PLs in Severe Human PAH—We next used IHC on paraffin-embedded human PAH lung tissue sections to investigate the presence of GrB within PLs and its association with ECs. We examined 57 PLs with three to 12 PLs per section (Table 1). Three of the 12 cases examined showed a lower number of PLs, Cases 6 and 9 (two PLs) and Case 5 (one PL). Based on the emerging clinical and biochemical evidence indicating that GrB can be expressed in other cell types of immune and non-immune origin such as smooth muscle cells (42) or synthesized perhaps by ECs in an

autocrine manner in PAH, we evaluated GrB presence by IHC using GrB Ab. GrB immunoreactivity was variable; frequently, prominent GrB staining was associated with the small PAs of PAH lungs, either perivascularly (Fig. 4*A*) or intraluminally (Fig. 4*C*), in most of the specimens. GrB was detected either in close proximity of ECs or co-localizing with CD31, used for positive identification of ECs (Fig. 4, *A* and *C*, panel c1). DAPI was used for nuclear staining. GrB co-localization or immediacy to ECs lining the pulmonary vessels with a diameter greater than 100 μm (medium and large vessels) was not common (Fig. 4*B*). Even for PAH specimens with less prominent GrB immunoreactivity (Fig. 4*D*), proximity of ECs of small PAs (Fig. 4*D*, panel d4) and co-localization with CD31 were detected (Fig. 4*D*, panels d4 and d4.1). GrB immunoreactivity was not detected on lung sections obtained from the available paraffin-embedded FD$_2$-Ctrl (Fig. 4*E*). Moreover, GrB immunoreactivity was detected in the microenvironment of concentric obliterative lesions frequently in close proximity of ECs (Fig. 4*G*, arrowheads and insets g1 and g2). H&E staining of the same lesion (Fig. 4*F*) revealed muscularization of the pulmonary arteriole in the center, increased adventitial tissue around the vessel, and some dilated thin walled vessels (arterioles or venules) at the very edge. A complex PL (Fig. 4*H*) shows GrB immuno-
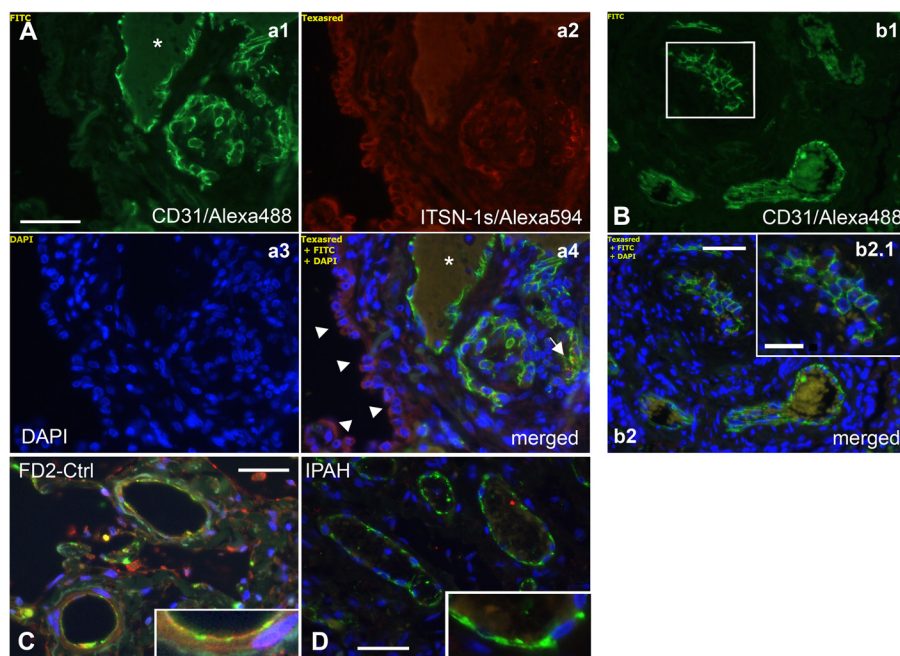
FIGURE 3. **ITSN is down-regulated in human PAH specimens.** Lung tissue sections of PAH (*A*, *B*, and *C*) and FD$_2$-Ctrl (*D*) were subjected to IHC using ITSN Ab and CD31 Ab. *Panel a1* illustrates that CD31 immunoreactivity of complex lesion with focal proliferation of several endothelial channels and partial destruction of the arterial wall. ITSN-1s pAb/anti-rabbit IgG-Alexa Fluor 594 staining (*panel a2*) is barely detected. DAPI staining (*panels a3* and *b2*) of the nuclei documents the hypercellularity and the concentric thickening/distribution of intimal cells. The merged image (*panel a4*) illustrates co-localization of CD31 with ITSN-1s remnants (*arrow*) in several ECs of the damaged arterial wall as well as ITSN-1s immunoreactivity associated with pulmonary epithelial cells (*arrowheads*). ITSN-1s immunoreactivity is barely detected at the level of a thin walled lymphatic in close proximity of the PL (*A*, *panels a1* and *a4*, *asterisk*). Clusters of proliferative ECs (*B*, *panel b1*, *circled area*) lacking ITSN-1s (*panels b2* and *b2.1*) surrounded by concentric intimal thickening are seen in the lumen of a small PA. *C*, *inset*, ITSN immunoreactivity is associated with ECs lining the blood vessels in FD$_2$-Ctrl. *D*, *inset*, low ITSN-1s staining in ECs lining the small blood vessels not yet detectably affected by remodeling in PAH specimen. The results are representative for 12 PAH cases. *Scale bars*, 50 (*A*, *B*, *C*, and *D*) and 25 μm (*panel b2.1*).

reactivity (*panel h1*) often in close proximity of ECs (*panels h2* and *h4*, *arrows*). DAPI staining of the nuclei revealed the typical concentric cell proliferation leading to luminal obliteration (Fig. 4*H*, *panel h3*). Thus, GrB is present in the milieu of the concentric obliterative lesions and PLs, which are temporally and etiologically related (43). Moreover, GrB can target pulmonary ECs, suggesting that GrB may cleave and down-regulate ITSN-1s protein in PAH lungs.

Myc-GrB-EH$_{ITSN}$ Has EC Proliferative Potential—Previous studies indicated that ITSN-1s or EH domains alone activate mitogenic signaling (20, 22). To address whether the GrB-EH$_{ITSN}$ has similar potential, we cloned it into pcDNA3.1Myc/His vector and expressed it in PAECs as described previously (19). Efficient expression of myc-GrB-EH$_{ITSN}$ protein was detected by Western blot of cell lysates using myc Ab at 48 h post-transfection (Fig. 5*A*). In addition, immunofluorescent staining of transfected ECs (Fig. 5*C*, *panel c1*) further demonstrated efficient protein expression and a subcellular distribution reminiscent of full-length ITSN-1s (19). No myc immunoreactivity was detected in untreated ECs (Fig. 5*B*). Next, control (Fig. 5*D*) and myc-GrB-EH$_{ITSN}$-transfected (Fig. 5*E*) ECs were subjected to a BrdU cell proliferation assay. Morphometric analyses indicated that GrB-EH$_{ITSN}$ expression caused a 40% increase in BrdU-positive cells compared with non-transfected ECs. ECs transfected with myc-tagged full-length ITSN-1s (myc-ITSN) were used for comparison. Only a modest increase (14%) was noted under these conditions (Fig. 5*F*), consistent with previous reports that within full-length ITSN-1s EH domains are under the inhibitory control of SH3A–E (20). Transfection with the empty vector did not affect the number of BrdU-positive ECs by reference to controls (not shown). Furthermore, we performed the MTT cell growth/proliferation assay to analyze biochemically the proliferation of the whole myc-GrB-EH$_{ITSN}$-transfected cell population. Cell growth was significantly higher in myc-GrB-EH$_{ITSN}$-transfected ECs compared with control cells (Fig. 5*G*). A growth curve was generated to relate the A_{570} values to the cell number per well. The extent of cell growth increase, calculated on three successive points on the curves, indicated a 50% increase in the number of myc-GrB-EH$_{ITSN}$-expressing ECs compared with controls (Fig. 5*H*). We concluded that the GrB-EH$_{ITSN}$ cleavage product has EC proliferative potential.

Myc-GrB-EH$_{ITSN}$ Specifically Activates p38^{MAPK}—Because expression of myc-GrB-EH$_{ITSN}$ increases EC proliferation and because ITSN-1s has been implicated in the regulation of Erk1/2^{MAPK} signaling due to its interaction with mSos, a guanine nucleotide exchange factor for Ras (20), we next addressed the effects of myc-GrB-EH$_{ITSN}$ on MAPK activation. Western blot with specific phospho-Erk1/2, JNK, and p38 Abs applied on lysates of control and myc-GrB-EH$_{ITSN}$-transfected cells indicated that myc-GrB-EH$_{ITSN}$ expression 48 h post-transfection activates p38^{MAPK} and has no effect on JNK (Fig. 6*A*). Myc-GrB-EH$_{ITSN}$-expressing cells, however, show decreased Erk1/2^{MAPK} activation, consistent with reports of a negative crosstalk from p38 to Erk1/2 that occurs only in non-transformed cells because p38 can enhance MEK dephosphorylation or up-regulate protein phosphatase 2A (44). Given some limited evidence regarding a role for ITSN-1 in the regulation of the PI3K/
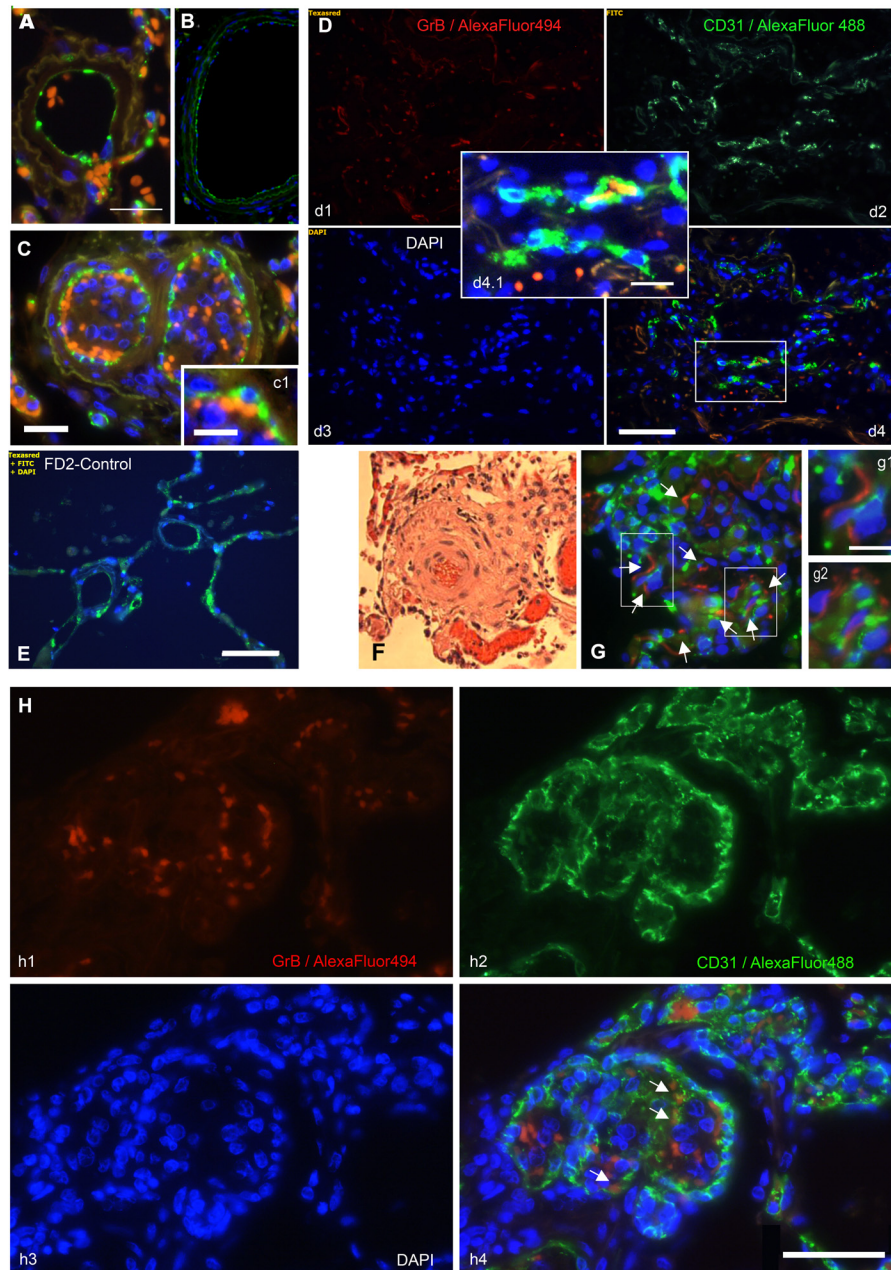
FIGURE 4. **GrB immunoreactivity in the PAH human lungs and the microenvironment of PLs.** Representative GrB/Alexa Fluor 594-CD31/Alexa Fluor 488 IHC of PAH human lung tissue sections illustrates close proximity between ECs and GrB immunoreactivity (*A*, *C*, and *D*); frequently GrB co-localizes with CD31 (*C*, *panel c1*) or was detected inside ECs labeled by CD31 (*panels d4* and *d4.1*). *B*, large PA from PAH specimen does not show GrB staining. *E*, FD$_2$-Ctrl lung sections do not show detectable GrB immunoreactivity. *F*, representative H&E staining of a concentric (onion skin) obliterative lesion in human PAH lungs. *G*, GrB (*arrows*) within the same obliterative lesion. *Arrowheads* in *G* and *insets g1* and *g2* (*boxed areas* in *G*) illustrate GrB immunoreactivity in close proximity of ECs. *H*, GrB/Alexa Fluor 594-CD31/Alexa Fluor 488 IHC of a large PL shows GrB immunoreactivity (*panel h1*), the high EC content (*panel h2*), and frequent presence of GrB in close proximity of CD31-labeled ECs (*panel h4*, *arrows*). DAPI staining of the nuclei is shown (*panel h3*). The results are representative for 12 PAH cases. Three independent IHC experiments were performed. *Scale bars*, 25 (*A*, *B*, and *C*), 50 (*D* and *E*), 10 (*panels c1* and *d4.1*), 40 (*F* and *G*), 20 (*panels g1* and *g2*), and 50 μm (*H*).

Akt signaling pathway in neurons (45), we also examined a possible role for GrB-EH$_{ITSN}$ in PI3K/Akt activity. No detectable changes in the phosphorylation status of these two kinases in ECs expressing the GrB-EH$_{ITSN}$ were noted (Fig. 6*A*).

Time course analysis of p38 activation in myc-GrB-EH$_{ITSN}$-transfected cells indicates strong p38^{MAPK} activation at 48 h post-transfection, the optimal time point for myc-GrB-EH$_{ITSN}$ expression; it remains persistent but decreases at 72 and 96 h post-transfection (Fig. 6*B*, *lanes c–e*). Myc-ITSN-trans-

fected ECs, used for comparison, showed minimal p38 activation (Fig. 6*B*, *lane b*). No p38 phosphorylation was detected under control conditions (Fig. 6*B*, *lane a*). To determine whether p38 activation accounts for proliferation of myc-GrB-EH$_{ITSN}$-transfected ECs, ECs were treated with a selective p38^{MAPK} inhibitor, SB203580 (10 μM), and then subjected to BrdU incorporation as above. The proliferative response of myc-GrB-EH$_{ITSN}$-transfected ECs was about 47% inhibited by reference to transfected cells without
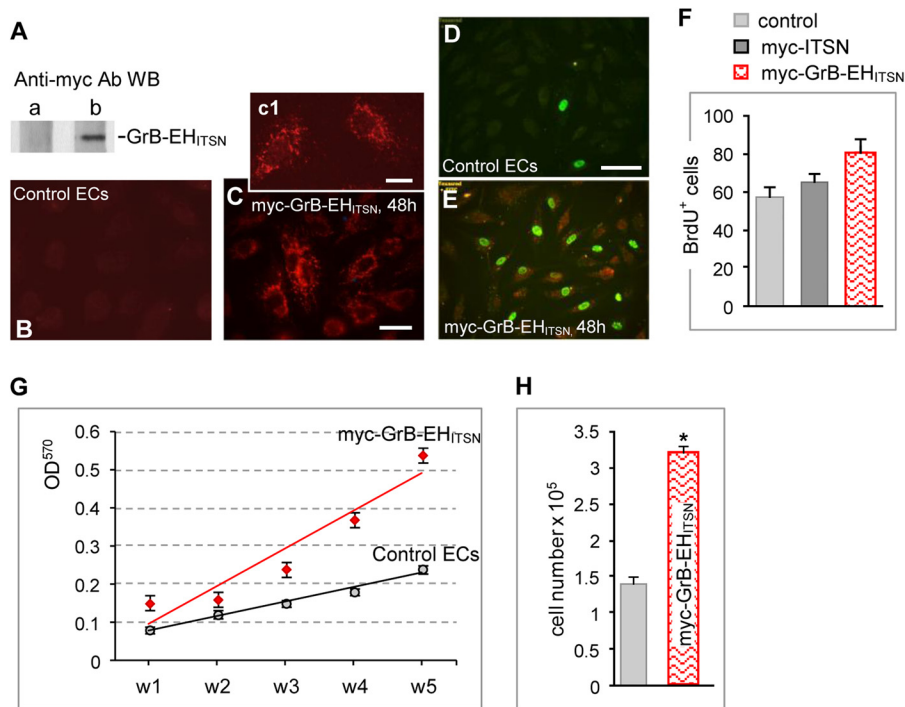
FIGURE 5. *A*, Myc-GrB-EH$_{ITSN}$ expression causes human PAEC proliferation. Lysates (70 μg of total protein/lane) of control (*lane a*) and myc-GrB-EH$_{ITSN}$-transfected ECs (*lane b*) were assessed for myc-GrB-EH$_{ITSN}$ protein expression by Western blotting (*WB*) using myc Ab. Immunofluorescent staining using myc pAb followed by anti-rabbit IgG-Alexa Fluor 594 of control (*B*) and myc-GrB-EH$_{ITSN}$-transfected cells (*C, panel c1*). Control (*D*) and myc-GrB-EH$_{ITSN}$-transfected (*E*) ECs 48 h post-transfection were incubated with BrdU reagent for 6 h at 37 °C. BrdU mAb/Alexa Fluor 488 were used to detect proliferating cells. *F*, quantification of BrdU-positive (BrdU$^+$) cells. The results are expressed as BrdU$^+$ ECs/high power field (50 power field images/experimental condition). Data are representative of three different experiments and were normalized per total number of cells counted. *G*, MTT assay applied on control and myc-GrB-EH$_{ITSN}$-transfected ECs 48 h post-transfection (*w*, well). *H*, quantification of the extent of myc-GrB-EH$_{ITSN}$-transfected EC proliferation. Data are presented as mean $\pm$ S.E. (*error bars*) from three to five independent experiments. *, $p < 0.05$ compared with the control. *Scale bars*, 20 (*B* and *C*), 10 (*panel c1*), and 50 μm (*D* and *E*).

SB203580 treatment (Fig. 6*C*). We concluded that myc-GrB-EH$_{ITSN}$ specifically activates p38^{MAPK}, and this activation accounts for its EC proliferative potential.

Myc-GrB-EH$_{ITSN}$ Expression Causes Nuclear Export of p38^{MAPK}—Morphological evaluation of p38^{MAPK} distribution in myc-GrB-EH$_{ITSN}$-expressing ECs by fluorescence microscopy revealed the presence of unphosphorylated p38^{MAPK} inside the nucleus, in the perinuclear area, and throughout the cytosol in both myc-GrB-EH$_{ITSN}$-transfected ECs and untreated cells (Fig. 6*D*, *panels d1* and *d2*). However, activated p38^{MAPK} was present predominantly in the cytosol of myc-GrB-EH$_{ITSN}$-expressing ECs (Fig. 6*E*, *panel e2*), consistent with previous reports demonstrating that activated p38 undergoes nuclear export and accumulates in the cytosol (46). Additionally, we observed that for some myc-GrB-EH$_{ITSN}$-transfected ECs phospho-p38^{MAPK} staining is brighter, suggesting either more efficient expression of the fragment in these cells or EC heterogeneity and enhanced response to myc-GrB-EH$_{ITSN}$ expression. Phospho-p38 staining in control ECs was low/barely detectable (Fig. 6*E*, *panel e1*). Nuclear export of p38^{MAPK} and prominent cytosolic phospho-p38 immunoreactivity were also detected in EC$_{PAH}$ (Fig. 6*E*, *panel e3*); the barely detectable GrB-EH$_{ITSN}$ expression by Western blot of EC$_{PAH}$ lysates may account for p38 activation in these cells. When paraffin-embedded lung tissue sections were subjected to phospho-p38 IHC (Fig. 6*F*), we detected phospho-p38 immunoreactivity within EC profiles labeled by CD31 Ab (Fig. 6*F*, *arrowheads*). Co-localization of phospho-p38 with DAPI nuclear staining was not

observed, consistent with activation and nuclear export of p38^{MAPK} into the cytosol of pulmonary ECs of PAH specimen. A complex PL comprising proliferative ECs shows phospho-p38 immunoreactivity (Fig. 6*G*). Given the high EC content, the phospho-p38/CD31 co-localization is significant. Activation of p38 was not detectable in the FD$_2$-Ctrl human lung (Fig. 6*H*).

Concurrent Expression of GrB/ITSN-1s Cleavage Products Affects p38/Erk1/2 Signaling—Because under physiological settings ITSN-1s cleavage by GrB generates two cleavage products, the N-terminal fragment with EC proliferative potential via p38 activation and the C-terminal product comprising the five SH3A–E domains with dominant negative effects on Ras/Erk1/2 signaling (21), we next addressed the effects of their concurrent expression on p38/Erk1/2^{MAPK} activity in the MCT mouse model (Fig. 7*A*). Mouse lung lysates were analyzed by Western blotting with specific phospho-p38 and Erk1/2 Abs followed by densitometry. We detected on average a 4-fold increase in activation of p38 in MCT-treated mice by comparison with untreated mice with a consistent 15% decrease in total p38 kinase expression. In addition, the Erk1/2 phosphorylation in MCT-treated mice was decreased by more than 3-fold compared with controls. Activation of p38 was more prominent in male mice, whereas Erk1/2 inhibition was more obvious in female mice, which are known to be more susceptible to MCT inflammatory effects. Analyses of p38/Erk1/2 activity were also carried out on human lung PAH tissue specimens sampled from two different locations (Fig. 7*B*). Densitometric analyses revealed a 4.8-fold increase in p38 activation and 4.5-fold
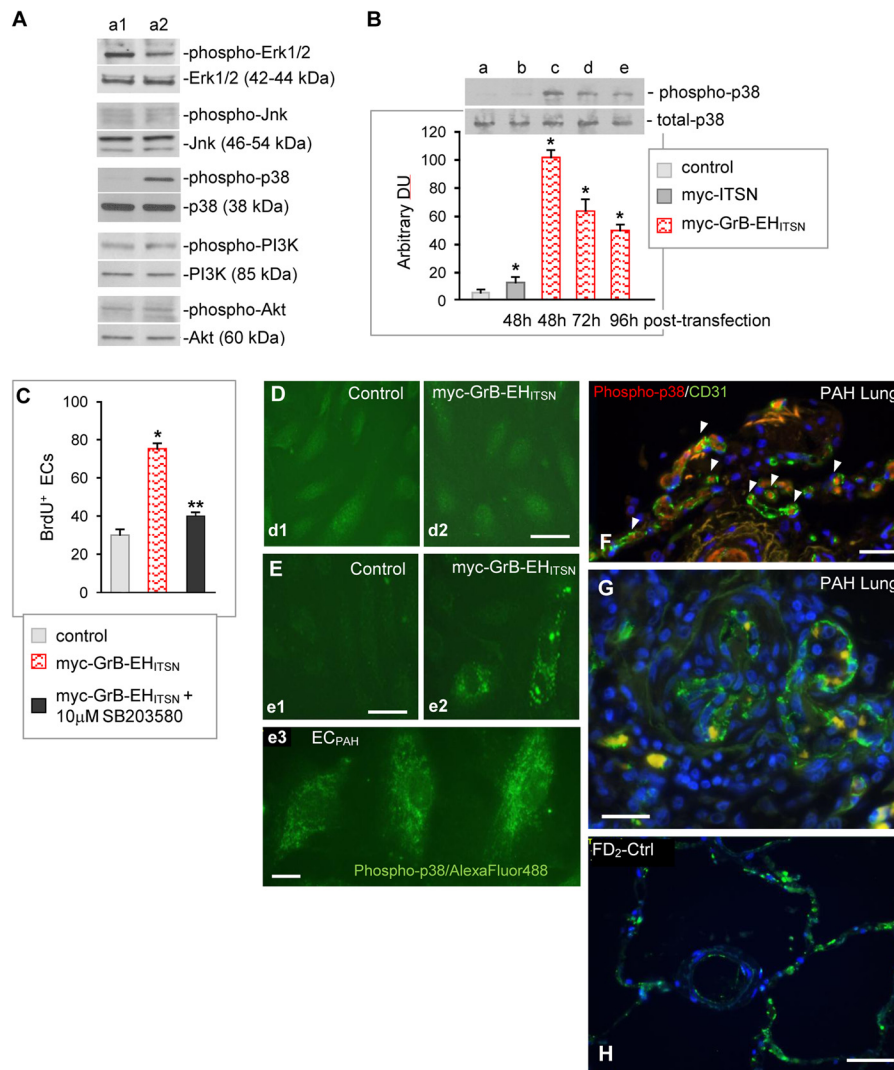
FIGURE 6. **Myc-GrB-EH$_{ITSN}$ specifically activates p38^{MAPK}.** *A*, lysates of control (*lane a1*) and myc-GrB-EH$_{ITSN}$-transfected ECs (*lane a2*) were assessed for Erk1/2^{MAPK}, JNK, PI3K/Akt, and p38 phosphorylation. *B*, time course of p38 activity in myc-GrB-EH$_{ITSN}$-expressing ECs (*lanes c–e*, 48, 72, and 96 h post-transfection) followed by densitometry. Non-transfected ECs (*lane a*) and myc-ITSN-transfected ECs 48 h post-transfection (*panel b*) were used for comparison. Densitometric values ±S.E. (*error bars*) are representative for three independent experiments. *C*, SB203580 abolishes the proliferative response in myc-GrB-EH$_{ITSN}$-expressing ECs. Data are shown as mean ± S.E. (*error bars*). *, $p < 0.01$; **, $p < 0.05$ compared with the control. *D*, immunofluorescent staining showing diffuse p38^{MAPK} staining both in control (*panel d1*) and myc-GrB-EH$_{ITSN}$-transfected ECs (*panel d2*). *E*, immunofluorescent staining for phospho-p38^{MAPK} in control (*panel e1*), myc-GrB-EH$_{ITSN}$-expressing ECs (*panel e2*), and EC$_{PAH}$ (B397; *panel e3*). *F* and *G*, phospho-p38/CD31 IHC on PAH human lung tissue sections, cases 10 and 3, respectively. *Arrowheads* point to phospho-p38 immunoreactivity within CD31-labeled EC profiles. *H*, phospho-p38/CD31 IHC on FD$_2$-Ctrl human lung tissue. *Scale bars*, 20 (*D* and *E*), 10 (*F*), and 25 μm (*G* and *H*). *DU*, densitometry units.

decrease in Erk1/2 activity. In addition, similar to the MCT mouse model, the decrease in total p38 protein expression was evident; actin confirmed the equal loading. Altogether, the observations are consistent with a role for GrB/ITSN-1s cleavage products in controlling the p38/Erk1/2^{MAPK} signaling activity.

Myc-GrB-EH$_{ITSN}$ Activates Elk-1 Transcription Factor and c-fos Immediate Early Response Gene—Because Elk-1, a nuclear transcription factor known to be downstream of p38^{MAPK}, stimulates the expression of immediate early response genes involved in cell growth and proliferation, its activation was evaluated by ELISA. Nuclear extracts of cells transfected with myc-GrB-EH$_{ITSN}$ showed ~50% higher Elk-1 activation compared with control and only 20% higher Elk-1 activation in ITSN-transfected ECs (Fig. 8A). Because the primary function of Elk-1 is the regulation of growth-related proteins, mainly c-Fos, we

evaluated c-Fos expression by Western blotting of the nuclear extracts (Fig. 8B). Densitometry indicated that cells expressing myc-GrB-EH$_{ITSN}$ showed a 4.8-fold increase in c-Fos expression compared with control cells, whereas those overexpressing full-length ITSN-1s showed a 3.2-fold increase, consistent with the recorded Elk-1 activation. Two transcription factors, Elk-1 and Sap-1a, bind efficiently with the serum response factor to the SRE of c-*fos* promoter to mediate gene expression in response to MAPK activation. To address whether there is any advantage between Elk-1 and Sap-1 in binding the SRE of c-*fos* promoter, nuclear extracts of control (Fig. 8C, *lane b*) and GrB-EH$_{ITSN}$-transfected ECs (Fig. 8C, *lanes c–g*) as well as biotin 3′-end-labeled DNA fragment containing the putative protein binding site from human c-*fos* gene (*lane a*) were subjected to a gel shift assay. Shift complexes were seen with the nuclear extracts of transfected ECs (*lanes c, d,* and *f*), reflecting the
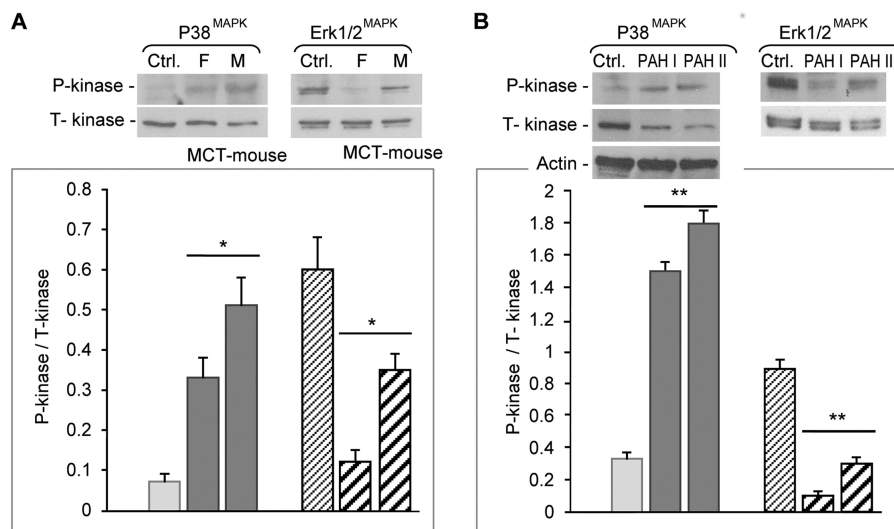
FIGURE 7. **Concurrent expression of GrB/ITSN-1s cleavage products results in a high p38/Erk1/2 activity ratio.** *A*, lysates of MCT-treated mouse lungs (70 μg of total protein) were resolved by SDS-PAGE, electrotransferred to nitrocellulose membranes, and further analyzed by Western blotting for phospho-p38 and phospho-Erk1/2 immunoreactivity. Total kinase was used as a loading control. Representative blots and corresponding densitometry (phosphokinase (*P-kinase*)/total kinase (*T-kinase*) ratio) are shown. The results of three independent experiments (three male (*M*) and three female (*F*) mice; 8-week MCT treatment) are expressed as mean $\pm$ S.E. (*error bars*). *, $p < 0.05$ *versus* control. *B*, human lung lysates (70 μg of protein) of FD$_1$-Ctrl and PAH tissue sampled from two different locations (PAH I and PAH II) were analyzed as above. Total kinase was used as a loading control. Given the decreased expression of p38 in PAH lung lysates, actin was further used to confirm equal protein loading. Representative blots and corresponding densitometric analyses of p38 and Erk1/2 phosphorylation are shown. $n = 3$. Data are expressed as mean $\pm$ S.E. (*error bars*). **, $p < 0.01$ compared with the control.

binding of a nuclear factor to the probe. The binding reaction was performed at room temperature (*lane c*) and 37 °C (*lane d*) with no detectable difference in the formation of shift complexes. This binding is specific because it was competed out with 100-fold excess unlabeled oligonucleotides probe (*lane e*). To determine whether the transcription factor in the shift complex was Elk-1 or Sap-1a, we performed the supershift assay in the presence of Abs to the C terminus of Elk-1 or Sap-1a; neither of them interfered with protein-DNA binding. The Ab to Elk-1 caused a supershift band (*lane g*), whereas the Ab to Sap-1a caused no supershift (*lane f*). No shift was detected when control ECs were analyzed (*lane b*).

To examine whether GrB-EH$_{ITSN}$ induces Elk-1 binding to c-*fos* SRE *in vivo*, we performed ChIP using Elk-1 Ab. Rabbit IgG was used as a control. The immunoprecipitate was subjected to DNA extraction and PCR to amplify the region encompassing the corresponding Elk-1 binding sites in the human c-*fos* SRE. GrB-EH$_{ITSN}$ significantly increased Elk-1 binding on the c-*fos* SRE in myc-GrB-EH$_{ITSN}$-expressing ECs (Fig. 8*D*). Based on these findings, we concluded that myc-GrB-EH$_{ITSN}$-mediated p38^{MAPK} activity specifically turns on Elk-1 transcription factor and c-*fos* gene.

DISCUSSION

This study has demonstrated that the proteolytic cleavage of ITSN-1s by GrB exerts complex effects on growth and proliferation of PAECs that are significant for formation of PLs in severe PAH. We have found that cytotoxic protease GrB cleaves the prosurvival protein ITSN-1s and generates two biologically active products with the N-terminal fragment possessing EC proliferative potential. ITSN-1s cleavage occurs at IDQD^{271}GK, a well conserved sequence among mammals, suggesting that during inflammatory processes associated with increased CD8$^+$ T-cells and GrB expression the ubiquitously expressed ITSN-1s protein is cleaved,

and as result, full-length protein expression is decreased. This is significant taking into account that ITSN-1s is a multifunctional protein and that chronic deficiency of ITSN-1s contributes to EC proliferation and vascular remodeling as well as lung malignancies (22, 23). The MCT-induced PAH mouse and rat models were used to demonstrate that the cytotoxic protease GrB cleaves ITSN-1s *in vivo*, leading to decreased full-length protein expression as well as the presence of the GrB-EH$_{ITSN}$ cleavage product. Although it is recognized that the response to MCT is variable among species, strains, and even animals because of differences in hepatic metabolism by cytochrome P450 (47), the 8-week MCT treatment induces PAH in the mouse model and allows enough time for the development of proliferative arteriopathy (30); rats apparently die of cardiac and renal dysfunction before the formation of occlusive vascular lesions (48). In addition, using human lung PAH specimens, we show that GrB immunoreactivity is associated with the small PAs and PLs and that ITSN-1s is significantly down-regulated compared with FD-Ctrl specimens. These observations are consistent with the idea that during PAH progression when T-cell inflammation is persistent GrB cleaves ITSN-1s and generates the N-terminal cleavage product with EC proliferative potential. This observation seems uncommon taking into account the well documented proapoptotic effects of GrB (14) and that EC is not a typical GrB target. During an inflammatory response, ECs lining the blood vessels are exposed to nonspecifically released GrB and perforin (9). Previous reports demonstrated that the proinflammatory EC dysfunction is associated with ITSN-1s down-regulation and Bcl-X$_L$ overexpression (4) and that Bcl-X$_L$ is able to suppress apoptotic cell death induced by ITSN-1s down-regulation (27) and GrB/perforin exposure (8). Although non-apoptotic pathways promoted by GrB and gain of function of the GrB cleavage fragments cannot be ruled out
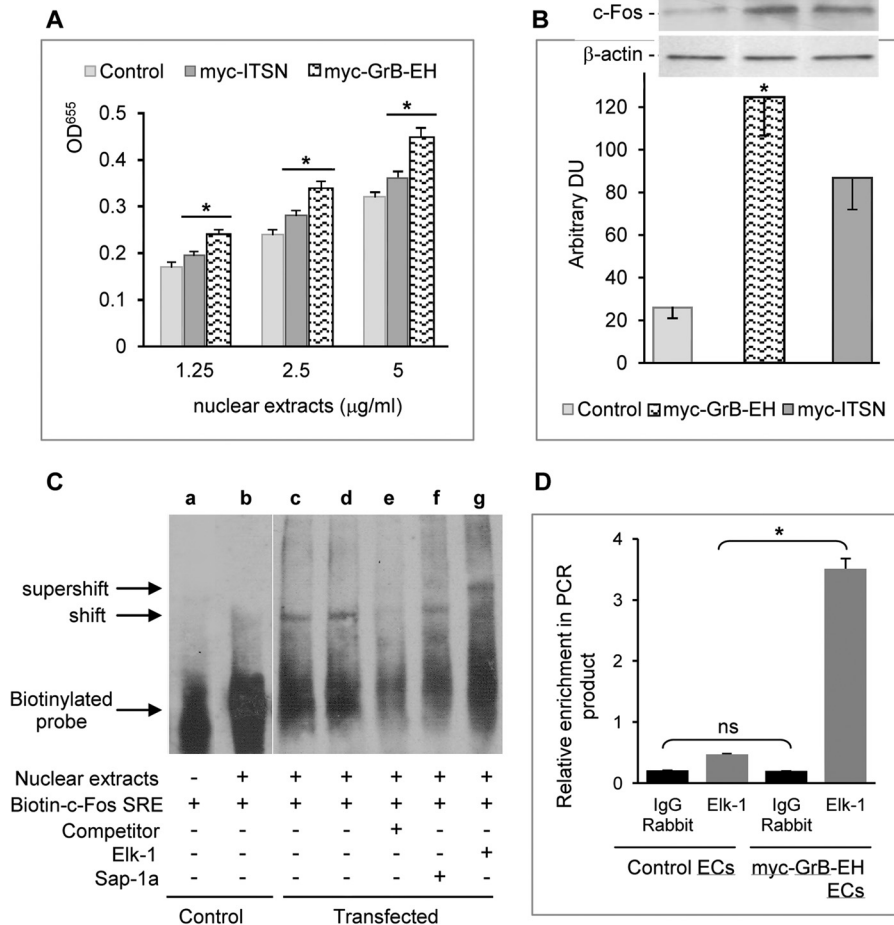
FIGURE 8. **Myc-GrB-EH activates Elk-1 transcription factor and cellular immediate early response gene *c-fos*.** *A*, nuclear extracts (three different concentrations) prepared from control, myc-ITSN-, and myc-GrB-EH$_{ITSN}$-transfected ECs were assayed for Elk-1 activity using an ELISA kit designed to detect only active Elk-1. Data are representative of three independent experiments performed in triplicates and are expressed as mean ± S.E. (*error bars*). *, *p* < 0.05 *versus* control. *B*, Western blot of nuclear extracts (45 μg/lane) from control, myc-GrB-EH$_{ITSN}$-, and myc-ITSN-transfected ECs using c-Fos Ab and consequent densitometric analysis. Data were normalized to β-actin. Data represent mean ± S.E. (*error bars*) from three different experiments. *, *p* < 0.05 *versus* control. *C*, a gel shift assay was used to analyze the *c-fos* SRE binding activity in control ECs and myc-GrB-EH$_{ITSN}$-transfected cells. All lanes have biotin-labeled *c-fos* probe containing the Elk-1 binding sequence. *Lane a*, biotin-labeled *c-fos* probe alone. Nuclear extract from transfected cells shows a shift of the *c-fos*·Elk-1 complex (*lanes c*, *d*, and *f*). This DNA·protein complex is not detected in control ECs (*lane b*) or in the presence of a 100-fold excess of unlabeled probe (*lane e*). In the presence of an Ab specific for Elk-1 protein, a supershift is detected in myc-GrB-EH$_{ITSN}$-transfected ECs (*lane g*). However, this supershifted complex is not detected in the presence of Sap-1a Ab (*lane f*). *D*, ChIP assay applied to control and myc-GrB-EH$_{ITSN}$-transfected ECs using Elk-1 Ab and rabbit IgG. Immunoprecipitated DNA samples were further amplified by quantitative RT-PCR. Data represent mean ± S.E. (*error bars*) from three different experiments. *, *p* < 0.01 *versus* control; *ns*, not statistically significant. *DU*, densitometry units.

as a possibility for EC survival, it is very likely that Bcl-X$_L$-mediated suppression of caspase activation induced by GrB (16) occurs during inflammation associated with PAH, and thus ECs are protected against GrB-induced apoptosis.

The C-terminal cleavage product, GrB-SH3A-E$_{ITSN}$, by sequestering mSos has dominant negative effects on Ras/Erk1/2^{MAPK} signaling (21) (Fig. 9). Worth mentioning is that the GrB-SH3A-E$_{ITSN}$ can also bind Smad2, which is able to bind SH3 domains of adaptor proteins such as AMSH-2 (associated molecule with the SH3 domain of STAM (signal transducing adaptor molecule); Ref. 49). If this occurs, the interaction may inhibit Smad2-dependent TGFβ signaling and augment EC proliferation. Although the two GrB cleavage products promote both proliferative and apoptotic signaling in lung ECs, the utilization of these signals appear to be cell type- (location of EC) and cell context-specific (heterogeneity of EC).

Recently, we have shown that chronic ITSN-1s deficiency in mouse lung in the absence of inflammation and thus without

GrB cleavage of ITSN-1 impairs TGFβ receptor 1/Smad-2,3/SARA (Smad anchor for receptor activation)-dependent signaling (22) to exert an EC proproliferative response. Thus, ITSN-1s deficiency may further augment the proliferative effects of the GrB-EH$_{ITSN}$ and contribute to PLs and vascular remodeling in severe PAH.

Under physiological conditions, the concurrent expression of the cleavage products results in a high p38/Erk1/2^{MAPK} activity ratio, which is critical for EC proliferation. It is possible that some ECs may take advantage of the growth potential, overcome death, and become hyperproliferative. The complexity of the cellular signaling and the temporal patterns of activation and regulatory feedback structures within the signaling network may further influence the p38/Erk1/2 activity ratio (40). The opposing effects of p38 activation on Erk1/2 (44) may further contribute to the high p38/Erk1/2^{MAPK} activity ratio (Fig. 9). Increasing evidence implicates p38^{MAPK} in the cell proliferation and vascular obliteration that characterize PAH (25,
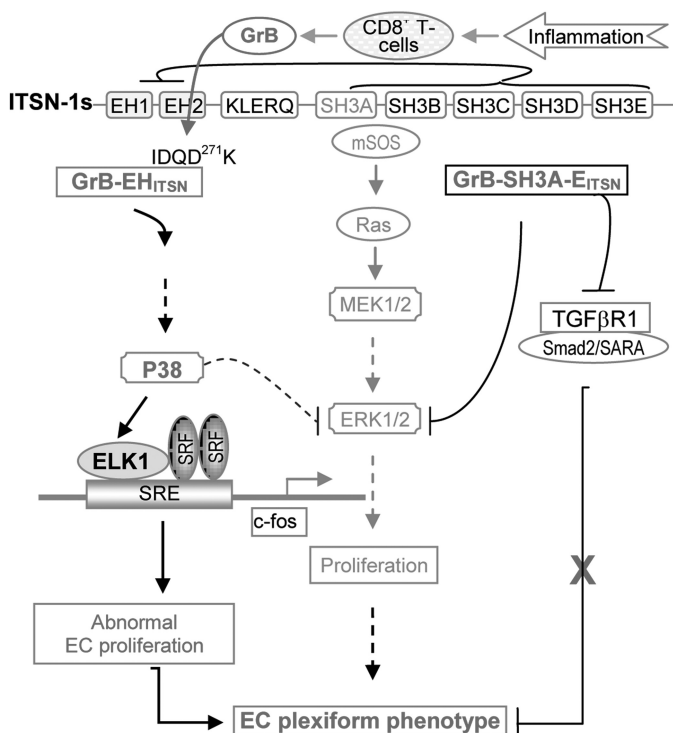
FIGURE 9. Diagram of the proposed GrB-EH$_{ITSN}$/p38^{MAPK}/Elk-1-mediated molecular mechanism resulting in the development of a proliferative/plexiform EC phenotype in severe PAH. The domain structure of full-length ITSN is shown. *KLERQ*, coiled coil domain. CD8$^+$ T-lymphocytes and increased GrB expression cause cleavage of ITSN at IDQD^{271}GK, generating an N-terminal cleavage product (GrB-EH$_{ITSN}$) and a C-terminal cleavage product (GrB-SH3A-E$_{ITSN}$). Because ITSN has only one cleavage site for GrB and is not a substrate for any caspases (PeptideCutter), the two cleavage products are generated in equimolar amounts. Both GrB/ITSN cleavage products are biologically active and interfere with the activity of two mitogen-activated protein kinases: GrB-EH$_{ITSN}$ activates p38, whereas GrB-SH3A-E$_{ITSN}$ has dominant negative effects on Ras/Erk1/2 survival signaling (21). In the context of full-length ITSN, EH domains are under the inhibitory control of SH3A–E (20). ITSN binds mSos and regulates GTP-Ras levels and thus downstream Erk1/2 survival signaling (*green font*). GrB-EH$_{ITSN}$ activates Elk-1 transcription factor via p38^{MAPK}. Sustained p38 activation and Elk-1 positive regulation of *c-fos* promoter favor the selection of a proliferative/plexiform EC phenotype. A negative cross-talk from p38 to Erk1/2 occurs because p38 can enhance MEK dephosphorylation or up-regulate protein phosphatase 2A (44). The C-terminal cleavage product (GrB-SH3A-E$_{ITSN}$) may perhaps interact with Smad2, recently shown to bind SH3 domains (49), causing ineffective assembly of TGFβ receptor 1 (*TGFβR1*)·Smad2·SARA (Smad anchor for receptor activation) signaling complex; deficient Smad2-dependent TGFβ signaling results in inhibition of its antiproliferative activity. *SRF*, serum response factor.

54, 55). However, the molecular mechanisms responsible are not well understood. We show that p38^{MAPK} activation mediates the proliferative potential of GrB-EH$_{ITSN}$; the activation of p38^{MAPK} is persistent and specific and implies nuclear export of activated kinase to the cytosol. In response to p38^{MAPK} activation, ECs proliferate, and the proliferation is abolished by chemical inhibition of p38 kinase. In this study, we included immunocyto- and -histochemical evidence of p38^{MAPK} activation in human PAH specimens: EC$_{PAH}$, cells that retain the PAH phenotype in culture, and lung tissue of PAH subjects. Both human specimens exhibited phospho-p38 immunoreactivity and nuclear export of the activated kinase into the cytosol as well as full-length ITSN-1s deficiency. Activation of p38 in EC$_{PAH}$ in the absence of GrB-mediated ITSN-1s cleavage can be caused by the alternatively spliced EH$_{ITSN}$, which is apparently present in these cells. These observations demonstrate

that ITSN-1s down-regulation, the presence of the N-terminal EH$_{ITSN}$ fragment with EC proliferative potential, and a high p38/Erk1/2 activity ratio are hallmarks of the stable EC plexiform phenotype in severe PAH.

The use of disease-free lung tissue as a control is challenging for cell signaling studies. Donor lung preservation from the time of procurement up until implantation in the recipient requires, in addition to the optimal preservation solution, storage temperature, inflation volume, and oxygen concentration, the use of pharmacological additives (*i.e.* prostaglandins and glucocorticoids) to enhance lung graft success (50–52). These pharmacological additives, lung transplant rejection, or perhaps associated disease may interfere with p38/Erk1/2^{MAPK} activity (53). Thus, the extent of kinase activation in these FD lungs should be cautiously read and used.

Another novel finding of this study is that we identified Elk-1 transcription factor as a specific downstream target of GrB-EH$_{ITSN}$-activated p38^{MAPK}. We and others (20) have noted that the EH domains of ITSN activate Elk-1, a member of the Ets (E twenty-six) ternary complex transcription factors known to stimulate the expression of immediate early response genes involved in cellular proliferation and apoptosis (56). Elk-1 is a target for both the mitogenic (Erk1/2) and stress-activated (p38 and JNK) mitogen-activated protein kinases. p38^{MAPK} is generally known as a stress kinase believed to mediate cell death (57, 58). Previous studies (59) and our work indicate, however, that p38 signaling may also be essential for cell survival and proliferation instead of death. Noteworthy is the fact that all bone morphogenetic protein type II receptor mutations underlying primary PAH demonstrate a gain of function involving up-regulation of p38^{MAPK}-dependent proproliferative pathways (55). Elk-1 positively regulates *c-fos* promoter activities (56, 60). The rapid induction of the *c-fos* gene is one of the initial events in stimulating cell proliferation by a variety of growth factors (61). Although our studies convincingly demonstrate a novel pathogenic ITSN-1s/p38-dependent signaling pathway accounting for the plexogenic EC phenotype in severe PAH, studies are still needed to show that ITSN-1s deficiency and the presence of EH$_{ITSN}$ induce PAH *in vivo*.

In summary, we have demonstrated that ITSN-1s deficiency and the GrB cleavage fragment with EC proliferative potential are important players in a novel p38^{MAPK}/Elk-1-dependent molecular mechanism underlying EC proliferation and abnormal vascular remodeling that characterizes PAH. Drugs preventing the GrB/ITSN cleavage or reducing the proliferative effect of GrB-EH$_{ITSN}$ can be used in combination therapies for specifically targeting this normally fatal disease with multifactorial etiology.

REFERENCES

1. Voelkel, N. F., Quaife, R. A., Leinwand, L. A., Barst, R. J., McGoon, M. D., Meldrum, D. R., Dupuis, J., Long, C. S., Rubin, L. J., Smart, F. W., Suzuki, Y. J., Gladwin, M., Denholm, E. M., and Gail, D. B. (2006) Right ventricular function and failure: report of a National Heart, Lung, and Blood Institute working group on cellular and molecular mechanisms of right heart failure. *Circulation* **114,** 1883–1891
2. Tuder, R. M., Marecki, J. C., Richter, A., Fijalkowska, I., and Flores, S. (2007) Pathology of pulmonary hypertension. *Clin. Chest Med.* **28,** 23–42
3. Masri, F. A., Xu, W., Comhair, S. A., Asosingh, K., Koo, M., Vasanji, A.,

Drazba, J., Anand-Apte, B., and Erzurum, S. C. (2007) Hyperproliferative apoptosis-resistant endothelial cells in idiopathic pulmonary arterial hypertension. *Am. J. Physiol. Lung Cell Mol. Physiol.* **293,** L548 –L554

4. Singla, S., Predescu, D., Bardita, C., Wang, M., Zhang, J., Balk, R. A., and Predescu, S. (2011) Pro-inflammatory endothelial cell dysfunction is associated with intersectin-1s down-regulation. *Respir. Res.* **12,** 46

5. Tu, L., Dewachter, L., Gore, B., Fadel, E., Dartevelle, P., Simonneau, G., Humbert, M., Eddahibi, S., and Guignabert, C. (2011) Autocrine fibroblast growth factor-2 signaling contributes to altered endothelial phenotype in pulmonary hypertension. *Am. J. Respir. Cell Mol. Biol.* **45,** 311–322

6. Huang, J., Wolk, J. H., Gewitz, M. H., and Mathew, R. (2012) Caveolin-1 expression during the progression of pulmonary hypertension. *Exp. Biol. Med.* **237,** 956 –965

7. Suzuki, Y. J., Nagase, H., Wong, C. M., Kumar, S. V., Jain, V., Park, A. M., and Day, R. M. (2007) Regulation of Bcl-xL expression in lung vascular smooth muscle. *Am. J. Respir. Cell Mol. Biol.* **36,** 678 – 687

8. MacDonald, G., Shi, L., Vande Velde, C., Lieberman, J., and Greenberg, A. H. (1999) Mitochondria-dependent and -independent regulation of granzyme B-induced apoptosis. *J. Exp. Med.* **189,** 131–144

9. Buzza, M. S., Hirst, C. E., Bird, C. H., Hosking, P., McKendrick, J., and Bird, P. I. (2001) The granzyme B inhibitor, PI-9, is present in endothelial and mesothelial cells, suggesting that it protects bystander cells during immune responses. *Cell. Immunol.* **210,** 21–29

10. Savai, R., Pullamsetti, S. S., Kolbe, J., Bieniek, E., Voswinckel, R., Fink, L., Scheed, A., Ritter, C., Dahal, B. K., Vater, A., Klussmann, S., Ghofrani, H. A., Weissmann, N., Klepetko, W., Banat, G. A., Seeger, W., Grimminger, F., and Schermuly, R. T. (2012) Immune and inflammatory cell involvement in the pathology of idiopathic pulmonary arterial hypertension. *Am. J. Respir. Crit. Care Med.* **186,** 897–908

11. Ars, C., Thurion, P., Delos, M., Sibille, Y., and Pilette, C. (2009) Small airway obstruction in severe pulmonary arterial hypertension correlates with increased airway CD8+ T-cells and fractalkine expression. *Eur. Respir. J.* **34,** 1494 –1496

12. Austin, E. D., Rock, M. T., Mosse, C. A., Vnencak-Jones, C. L., Yoder, S. M., Robbins, I. M., Loyd, J. E., and Meyrick, B. O. (2010) T lymphocyte subset abnormalities in the blood and lung in pulmonary arterial hypertension. *Respir. Med.* **104,** 454 – 462

13. Wang, W., Wang, Y. L., Chen, X. Y., Li, Y. T., Hao, W., Jin, Y. P., and Han, B. (2011) Dexamethasone attenuates development of monocrotaline-induced pulmonary arterial hypertension. *Mol. Biol. Rep.* **38,** 3277–3284

14. Ewen, C. L., Kane, K. P., and Bleackley, R. C. (2012) A quarter century of granzymes. *Cell Death Differ.* **19,** 28 –35

15. Susanto, O., Trapani, J. A., and Brasacchio, D. (2012) Controversies in granzyme biology. *Tissue Antigens* **80,** 477– 487

16. Loeb, C. R., Harris, J. L., and Craik, C. S. (2006) Granzyme B proteolyzes receptors important to proliferation and survival, tipping the balance towards apoptosis. *J. Biol. Chem.* **281,** 28326 –28335

17. Guipponi, M., Scott, H. S., Chen, H., Schebesta, A., Rossier, C., and Antonarakis, S. E. (1998) Two isoforms of a human intersectin (ITSN) protein are produced by brain-specific alternative splicing in a stop codon. *Genomics* **53,** 369 –376

18. Hussain, N. K., Yamabhai, M., Ramjaun, A. R., Guy, A. M., Baranes, D., O'Bryan, J. P., Der, C. J., Kay, B. K., and McPherson, P. S. (1999) Splice variants of intersectin are components of the endocytic machinery in neurons and nonneuronal cells. *J. Biol. Chem.* **274,** 15671–15677

19. Predescu, S. A., Predescu, D. N., Timblin, B. K., Stan, R. V., and Malik, A. B. (2003) Intersectin regulates fission and internalization of caveolae in endothelial cells. *Mol. Biol. Cell* **14,** 4997–5010

20. Adams, A., Thorn, J. M., Yamabhai, M., Kay, B. K., and O'Bryan, J. P. (2000) Intersectin, an adaptor protein involved in clathrin-mediated endocytosis, activates mitogenic signaling pathways. *J. Biol. Chem.* **275,** 27414 –27420

21. Tong, X. K., Hussain, N. K., Adams, A. G., O'Bryan, J. P., and McPherson, P. S. (2000) Intersectin can regulate the Ras/MAP kinase pathway independent of its role in endocytosis. *J. Biol. Chem.* **275,** 29894 –29899

22. Bardita, C., Predescu, D., Justice, M. J., Petrache, I., and Predescu, S. (2013) *In vivo* knockdown of intersectin-1s alters endothelial cell phenotype and causes microvascular remodeling in the mouse lungs. *Apoptosis* **18,** 57–76

23. Predescu, D., Zhang, J., Patel, M., Bardita, C., and Predescu, S. (2012)

24. Downregulation of intersectin-1s in human lung cancer may contribute to tumorigenesis. *Cancer Res.* **72,** Suppl. 1, Abstr. 3264

24. Derynck, R., and Zhang, Y. E. (2003) Smad-dependent and Smad-independent pathways in TGF-β family signalling. *Nature* **425,** 577–584

25. Yang, X., Long, L., Southwood, M., Rudarakanchana, N., Upton, P. D., Jeffery, T. K., Atkinson, C., Chen, H., Trembath, R. C., and Morrell, N. W. (2005) Dysfunctional Smad signaling contributes to abnormal smooth muscle cell proliferation in familial pulmonary arterial hypertension. *Circ. Res.* **96,** 1053–1063

26. Welsh, D. J., Peacock, A. J., MacLean, M., and Harnett, M. (2001) Chronic hypoxia induces constitutive p38 mitogen-activated protein kinase activity that correlates with enhanced cellular proliferation in fibroblasts from rat pulmonary but not systemic arteries. *Am. J. Respir. Crit. Care Med.* **164,** 282–289

27. Predescu, S. A., Predescu, D. N., Knezevic, I., Klein, I. K., and Malik, A. B. (2007) Intersectin-1s regulates the mitochondrial apoptotic pathway in endothelial cells. *J. Biol. Chem.* **282,** 17166 –17178

28. Comhair, S. A., Xu, W., Mavrakis, L., Aldred, M. A., Asosingh, K., and Erzurum, S. C. (2012) Human primary lung endothelial cells in culture. *Am. J. Respir. Cell Mol. Biol.* **46,** 723–730

29. Knezevic, I., Predescu, D., Bardita, C., Wang, M., Sharma, T., Keith, B., Neamu, R., Malik, A. B., and Predescu, S. (2011) Regulation of dynamin-2 assembly-disassembly and function through the SH3A domain of intersectin-1s. *J. Cell. Mol. Med.* **15,** 2364 –2376

30. George, J., and D'Armiento, J. (2011) Transgenic expression of human matrix metalloproteinase-9 augments monocrotaline-induced pulmonary arterial hypertension in mice. *J. Hypertens.* **29,** 299 –308

31. Predescu, D. N., Neamu, R., Bardita, C., Wang, M., and Predescu, S. A. (2012) Impaired caveolae function and upregulation of alternative endocytic pathways induced by experimental modulation of intersectin-1s expression in mouse lung endothelium. *Biochem. Res. Int.* **2012,** 672705

32. Aliotta, J. M., Keaney, P. J., Warburton, R. R., DelTatto, M., Dooner, M. S., Passero, M. A., Quesenberry, P. J., and Klinger, J. R. (2009) Marrow cell infusion attenuates vascular remodeling in a murine model of monocrotaline-induced pulmonary hypertension. *Stem Cells Dev.* **18,** 773–782

33. Seta, F., Rahmani, M., Turner, P. V., and Funk, C. D. (2011) Pulmonary oxidative stress is increased in cyclooxygenase-2 knockdown mice with mild pulmonary hypertension induced by monocrotaline. *PLoS One* **6,** e23439

34. Hostetter, D. R., Loeb, C. R., Chu, F., and Craik, C. S. (2007) Hip is a pro-survival substrate of granzyme B. *J. Biol. Chem.* **282,** 27865–27874

35. Kitamura, Y., Hashimoto, S., Mizuta, N., Kobayashi, A., Kooguchi, K., Fujiwara, I., and Nakajima, H. (2001) Fas/FasL-dependent apoptosis of alveolar cells after lipopolysaccharide-induced lung injury in mice. *Am. J. Respir. Crit. Care Med.* **163,** 762–769

36. Maxwell, J. R., Ruby, C., Kerkvliet, N. I., and Vella, A. T. (2002) Contrasting the roles of costimulation and the natural adjuvant lipopolysaccharide during the induction of T cell immunity. *J. Immunol.* **168,** 4372– 4381

37. Haies, D. M., Gil, J., and Weibel, E. R. (1981) Numerical and dimensional characteristics of parenchymal cell population. *Am. Rev. Respir. Dis.* **123,** 533–541

38. Gil, J. (1982) Alveolar wall relations. *Ann. N.Y. Acad. Sci.* **384,** 31– 43

39. Shi, R., Yang, J., Jaramillo, A., Steward, N. S., Aloush, A., Trulock, E. P., Alexander Patterson, G., Suthanthiran, M., and Mohanakumar, T. (2004) Correlation between interleukin-15 and granzyme B expression and acute lung allograft rejection. *Transpl. Immunol.* **12,** 103–108

40. Clément, M. V., Legros-Maïda, S., Israël-Biet, D., Carnot, F., Soulié, A., Reynaud, P., Guillet, J., Gandjbakch, I., and Sasportes, M. (1994) Perforin and granzyme B expression is associated with severe acute rejection. Evidence for in situ localization in alveolar lymphocytes of lung-transplanted patients. *Transplantation* **57,** 322–326

41. Kropyvko, S., Gerasymchuk, D., Skrypkina, I., Dergai, M., Dergai, O., Nikolaienko, O., Rynditch, A., and Tsyba, L. (2010) Structural diversity and differential expression of novel human intersectin 1 isoforms. *Mol. Biol. Rep.* **37,** 2789 –2796

42. Hiebert, P. R., and Granville, D. J. (2012) Granzyme B in injury, inflammation, and repair. *Trends Mol. Med.* **18,** 732–741

43. Cool, C. D., Kennedy, D., Voelkel, N. F., and Tuder, R. M. (1997) Patho-

genesis and evolution of plexiform lesions in pulmonary hypertension associated with scleroderma and human immunodeficiency virus infection. *Hum. Pathol.* **28,** 434–442

44. Fey, D., Croucher, D. R., Kolch, W., and Kholodenko, B. N. (2012) Cross-talk and signaling switches in mitogen-activated protein kinase cascades. *Front. Physiol.* **3,** 355

45. Das, M., Scappini, E., Martin, N. P., Wong, K. A., Dunn, S., Chen, Y. J., Miller, S. L., Domin, J., and O'Bryan, J. P. (2007) Regulation of neuron survival through an intersectin-phosphoinositide 3'-kinase C2β-AKT pathway. *Mol. Cell. Biol.* **27,** 7906–7917

46. Ben-Levy, R., Hooper, S., Wilson, R., Paterson, H. F., and Marshall, C. J. (1998) Nuclear export of the stress-activated protein kinase p38 mediated by its substrate MAPKAP kinase-2. *Curr. Biol.* **8,** 1049–1057

47. Gomez-Arroyo, J. G., Farkas, L., Alhussaini, A. A., Farkas, D., Kraskauskas, D., Voelkel, N. F., and Bogaard, H. J. (2012) The monocrotaline model of pulmonary hypertension in perspective. *Am. J. Physiol. Lung Cell Mol. Physiol.* **302,** L363–L369

48. Abe, K., Toba, M., Alzoubi, A., Ito, M., Fagan, K. A., Cool, C. D., Voelkel, N. F., McMurtry, I. F., and Oka, M. (2010) Formation of plexiform lesions in experimental severe pulmonary arterial hypertension. *Circulation* **121,** 2747–2754

49. Ibarrola, N., Kratchmarova, I., Nakajima, D., Schiemann, W. P., Moustakas, A., Pandey, A., and Mann, M. (2004) Cloning of a novel signaling molecule, AMSH-2, that potentiates transforming growth factor beta signaling. *BMC Cell Biol.* **5,** 2

50. Cypel, M., and Keshavjee, S. (2013) Expanding lung donation: the use of uncontrolled non-heart beating donors. *Eur. J. Cardiothorac. Surg.* **43,** 419–420

51. Venkateswaran, R. V., Patchell, V. B., Wilson, I. C., Mascaro, J. G., Thompson, R. D., Quinn, D. W., Stockley, R. A., Coote, J. H., and Bonser, R. S. (2008) Early donor management increases the retrieval rate of lungs for transplantation. *Ann. Thorac. Surg.* **85,** 278–286

52. de Perrot, M., Fischer, S., Liu, M., Jin, R., Bai, X. H., Waddell, T. K., and Keshavjee, S. (2001) Prostaglandin E1 protects lung transplants from ischemia-reperfusion injury: a shift from pro- to anti-inflammatory cytokines. *Transplantation* **72,** 1505–1512

53. Wuyts, W. A., Vanaudenaerde, B. M., Dupont, L. J., Van Raemdonck, D. E., Demedts, M. G., and Verleden, G. M. (2005) Interleukin-17-induced interleukin-8 release in human airway smooth muscle cells: role for mitogen-activated kinases and nuclear factor-κB. *J. Heart Lung Transplant.* **24,** 875–881

54. Mortimer, H. J., Peacock, A. J., Kirk, A., and Welsh, D. J. (2007) p38 MAP kinase: essential role in hypoxia-mediated human pulmonary artery fibroblast proliferation. *Pulm. Pharmacol. Ther.* **20,** 718–725

55. Rudarakanchana, N., Flanagan, J. A., Chen, H., Upton, P. D., Machado, R., Patel, D., Trembath, R. C., and Morrell, N. W. (2002) Functional analysis of bone morphogenetic protein type II receptor mutations underlying primary pulmonary hypertension. *Hum. Mol. Genet.* **11,** 1517–1525

56. Oikawa, T. (2004) ETS transcription factors: possible targets for cancer therapy. *Cancer Sci.* **95,** 626–633

57. Han, J. Y., Jeong, J. Y., Lee, Y. K., Roh, G. S., Kim, H. J., Kang, S. S., Cho, G. J., and Choi, W. S. (2006) Suppression of survival kinases and activation of JNK mediate ethanol-induced cell death in the developing rat brain. *Neurosci. Lett.* **398,** 113–117

58. Hui, L., Bakiri, L., Stepniak, E., and Wagner, E. F. (2007) p38α: a suppressor of cell proliferation and tumorigenesis. *Cell Cycle* **6,** 2429–2433

59. Thornton, T. M., and Rincon, M. (2009) Non-classical p38 map kinase functions: cell cycle checkpoints and survival. *Int. J. Biol. Sci.* **5,** 44–51

60. Price, M. A., Rogers, A. E., and Treisman, R. (1995) Comparative analysis of the ternary complex factors Elk-1, SAP-1a and SAP-2 (ERP/NET). *EMBO J.* **14,** 2589–2601

61. Gurland, G., Ashcom, G., Cochran, B. H., and Schwartz, J. (1990) Rapid events in growth hormone action. Induction of c-fos and c-jun transcription in 3T3-F442A preadipocytes. *Endocrinology* **127,** 3187–3195